LAPPEENRANTA UNIVERSITY OF TECHNOLOGY
LUT School of Energy Systems
LUT Mechanical Engineering

Ekaterina Menshova

DEVELOPMENT OF LABVIEW PLATFORM FOR LOWER LEVEL SUBSYSTEMS OF ROS-OPERATED MOBILE ASSEMBLY ROBOT

Examiners: Professor Heikki Handroos
D. Sc. Tech. Eng. Hamid Roozbahani

ABSTRACT

Lappeenranta University of Technology
LUT School of Energy Systems
LUT Mechanical Engineering

Ekaterina Menshova

Development of LabVIEW Platform for Lower Level Subsystems of ROS-Operated Mobile Assembly Robot

Master's thesis

2017

65 pages, 31 figures and 8 tables

Examiners: Professor Heikki Handroos
D. Sc. (Tech.) Hamid Roozbahani

Keywords: low level control, sensors, temperature sensor, temperature control system, inertial measurement unit, Kalman filter, ultrasonic sensor, LabVIEW, real-time control

The problem of the repair, assembly or holding something in hazardous or dangerous for human beings environment has a great importance. The project of the Mobile Assembly Robot is suggested by the Laboratory of Intelligent Machines in Lappeenranta University of Technology as a solution of that problem. One of the essential aims of the robot is the sensorial connection with the space around it and monitoring the state of the robot itself. Development of the sensor monitoring and robot tools remote control system is the goal of the thesis. Devices used in the project: temperature sensors, fans, ultrasonic distance sensors, a lamp, inertial sensor are described as well as the Kalman filtering algorithm. Theoretical physical principles of sensors work are implemented into developed program in LabVIEW software. Communication between sensors mounted on the robot and the control station of the robot was set. Program software is developed for processing signals from sensors and sending information to devices onboard the robot. The result of the master thesis is the intuitive user interface of all low-level subsystems combined together. The interface demonstrates temperature of the robot under the cover, distance to obstacles, acceleration, angular velocity and Euler angles of the robot in the real-time mode.

ACKNOWLEDGEMENTS

I would like to express gratitude to my supervisor Hamid Roozbahani for his advices and support, Professor Heikki Handroos for opportunity to work in a team of a Mobile Assembly Robot project. As well, I would like to thank Juha Koivisto and Mikko Rikkonen for their invaluable help. Moreover, I want to mention my colleagues from Mobile Robot project team Miguel Cordero Sánchez, Chloé Nativel, Efim Poberezkin, Henri Kauppila and María Artigas Alfonso. My friends thank you for an unforgettable experience of working together.

Ekaterina Menshova

Ekaterina Menshova

Lappeenranta 19.3.2017

TABLE OF CONTENTS

LIST OF SYMBOLS AND ABBREVIATIONS

A	Constant coefficient of resistance-temperature relation [$°C^{-1}$]
$\mathbf{A_0}$	Linear acceleration vector
A_{0x}	Linear acceleration in *Ox* direction [m/s^2]
A_{0y}	Linear acceleration in *Oy* direction [m/s^2]
A_{0z}	Linear acceleration in *Oz* direction [m/s^2]
B	Constant coefficient of resistance-temperature relation [$°C^{-2}$]
$\mathbf{B}_k$	Control matrix
C	Constant coefficient of resistance-temperature relation [$°C^{-4}$]
c	Speed of the sound [m/s^2]
$\mathbf{F}$	Force vector in vibratory gyroscope
f	Amplitude of excitation force [N]
$f(.)$	Transition function [-]
$\mathbf{F}_k$	State-transition matrix
$\mathbf{F}_{k-1}$	State-transition matrix for the moment *k*-1
F_x	Force vector projection on *x*-axis [N]
F_y	Force vector projection on *y*-axis [N]
F_z	Force vector projection on *z*-axis [N]
$\mathbf{H}_k$	Observation matrix
$h(.)$	Observation function [-]
$\mathbf{I}$	Identity matrix
I_0	Continuous output current [A]
$\mathbf{K}_k$	Kalman optimal matrix of gain factors
k	Clock cycle of the filter operation [-]
m	Mass of the object in the vibratory gyroscope [kg]
N	Mean of distribution [-]
O	Origin of coordinates
Ox	Axis of the non-inertial reference frame

Oy	Axis of the non-inertial reference frame
Oz	Axis of the non-inertial reference frame
$\mathbf{P}_{k\|k}$	Posteriori error covariance matrix
$\mathbf{P}_{k\|k-1}$	Covariance matrix for the predicted state vector
$\mathbf{P}_{k-1\|k-1}$	Posteriori error covariance matrix for the moment k-1
$\mathbf{Q}_k$	Covariance of the process noise matrix
$\mathbf{Q}_{k-1}$	Covariance of the process noise matrix for the moment k-1
$\mathbf{r}$	Coordinate vector of the mass in the non-inertial reference frame
$\ddot{\mathbf{r}}$	Acceleration vector of the mass in the non-inertial reference frame
R_0	Resistance at 0°C [Ω]
R_{100}	Resistance at 100°C [Ω]
R_{out}	Typical output impedance [Ω]
$\mathbf{R}_k$	Covariance of observation noise matrix
r_s	Distance between an ultrasound sensor and an obstacle [m]
R_T	Resistance at the temperature T°C [Ω]
$\mathbf{S}_k$	Covariance matrix for the deviation vector
T	Temperature of the environment [°C]
t	Time from the moment of sending sound and receiving it back [s]
$\mathbf{u}_k$	Control vector
$\mathbf{u}_{k-1}$	Control vector for the moment k-1
V_0	Output voltage [V]
$\mathbf{v}_k$	Gaussian white noise
V_{sup}	External power supply voltage [V]
$\mathbf{w}_k$	Normal random process
x	Mass coordinate in x-direction [m]
$\mathbf{x}_k$	State vector at the moment k
$\hat{\mathbf{x}}_k$	Estimate of the state vector at the moment k
$\mathbf{x}_{k-1}$	State vector at the moment k-1

$\hat{\mathbf{x}}_{k\|k}$	Posteriori estimation vector at the moment *k* considering measurements from the beginning up to the moment *k*
$\hat{\mathbf{x}}_{k\|k-1}$	Posteriori estimation vector at the moment *k* considering measurements from the beginning up to the moment *k*-1
$\hat{\mathbf{x}}_{k-1\|k-1}$	Posteriori estimation vector at the moment *k*-1 considering measurements from the beginning up to the moment *k*-1
$\hat{\mathbf{x}}_{n\|m}$	Estimation of the true vector **x** at the moment *n* considering measurements from the beginning up to the moment *m*
xyz	Non-inertial reference frame for accelerometer and gyroscope
y	Mass coordinate in *y*-direction [m]
$\tilde{\mathbf{y}}_k$	Deviation of the observation obtained at step k
z	Mass coordinate in *z*-direction [m]
$\mathbf{z}_k$	Observation vector
α_{rt}	Resistance-temperature relation coefficient [$\Omega/(\Omega\cdot°\mathrm{C})$]
$\xi\eta\zeta$	Inertial reference frame for accelerometer and gyroscope
ρ	Coordinate vector of the mass in the inertial reference frame
$\ddot{\boldsymbol{\rho}}$	Acceleration vector of the mass in the inertial reference frame
Ω	Angular velocity vector
Ω_x	Angular velocity around *Ox* [rad/s]
Ω_y	Angular velocity around *Oy* [rad/s]
Ω_z	Angular velocity around *Oz* [rad/s]
ω	Natural frequency of ideal angle gyroscope [rad/s]
ω_d	Frequency of the sinusoidal waveform [rad/s]
ω_x	Natural frequency related to *Ox* axis [rad/s]
ω_y	Natural frequency related to *Oy* axis [rad/s]
ACK	Acknowledge
ADC	Analog to Digital Converter

C	Compact (about series module for compact controllers by National Instrument)
CPU	Central Processing Unit
cRIO	Compact Reconfigurable Input Output
FPGA	Field Programmable Gate Arrays
GNSS	Global Navigation Satellite System
GPS	Global Positioning System
I/O	Input/Output
IMU	Inertial Measurement Unit
INS	Inertial Navigation System
LabVIEW	Laboratory Virtual Instrumentation Engineering Workbench
MAX	Measurement & Automation Explorer
MEMS	Microelectromechanical Systems
NACK	Negative Acknowledge
NI	National Instrument
ROS	Robot Operating System
RS232	Recommended Standard 232
RTD	Resistance Temperature Detector
SD	Secure Digital
UART	Universal Asynchronous Receiver-Transmitter
VI	Virtual Instrument

1 INTRODUCTION

A hierarchical structure in robotics control is an idea of different functional levels implementation in the completely robotic system. A level segregation is made by functional and physical separation of robot components. (Siciliano et al. 2010, p. 233.)

Low-level subsystems consist of parts working in direct contact with environment. Examples of low levels are actuators, drivers, sensors, input/output devices. Higher-level subsystems include computers capable to manage data from low levels, solve kinematics and dynamics and make decision about further control of the robot.

The focus of the work is lower level subsystems as an inertial sensor, a temperature sensor and a distance sensor. According to abovementioned information about low-level systems, the purpose of all sensing devices is to obtain connection of a robotic mechanism with space around it.

Knowledge of low-level subsystems control has a great importance for implementation of whole control architecture to the result of engineering project. In recent years, there have been many papers describing low-level control systems in robotics. Evidence of that fact is demonstrated on an analyze chart on Figure 1. Researches describing low-level subsystems have been reported since 1975. However, that field of engineering sciences has received considerable attention just from 2013 until nowadays.

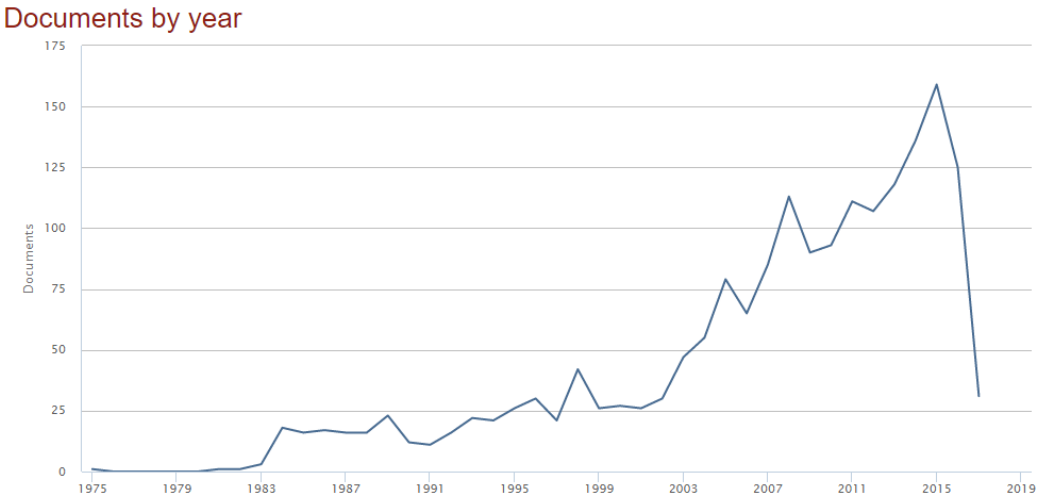

Figure 1. Number of publications per year by request "low level control" (Scopus 2017).

The general features of sensors as components of low-level subsystems are well known. Phenomenon of temperature estimation, distance determination, accelerometer and gyroscope assessment methods are generally accepted.

Low-level control system for mobile robot with Mecanum wheels has been presented in literature (Comansolivas et al. 2017). Robust controller was designed, tested and implemented by Comansolivas et al. (2017). An angle sensor utilization and measurement module of forces applied to flexible anthropomorphic robot hand are described by researchers (Martin et al. 2004, p. 517-532). Moreover, work of sensor and actuator subsystems was simulated by Martin et al. (2004, p. 517-532) for further usage of obtained results in development of robot control system. Implementation of FPGA (Field Programmable Gate Arrays) based approach for designing of low-level control for a robotic system was introduced by Falsig and Soerensen (2010, p. 6119-6124). Aim of the suggested method was an improvement of flexibility parameters of a low-level system control.

Development of temperature control systems was a purpose of researches presented by Heller and Youcef-Toumi (2014, p. 3335-3340). They suggested using a closed-loop control system for monitoring a temperature level and as a result improvement-operating properties of robotic system.

A large body of data concerning distance measurement sensors in robotics has been reported. Researches and experiments of a mobile robot with a control system based on ultrasonic distance sensors work were held by Chu (2015, p. 1238-1240) in South Korea. According to Korean researcher, sensors were implemented on NI (National Instrument) cRIO (Compact Reconfigurable Input Output) controller on a board of an Omni-directional mobile robot. Experiments showed effective performance of the system.

Inertial sensors were utilized for development of a navigation system in a mobile robot, as described by Qazizada and Pivarčiová (2016, p. 404-413). According to them, accelerometer and gyroscope data was included into calculation algorithm for detection of the mobile robot in the environment. Integrated acceleration and angular velocity allow determining position and orientation of a system in a space.

Although abovementioned studies and papers describe theoretical background, experiments and simulations, they did not include development of a user interface system for monitoring and control of a group of sensors.

Despite the importance of usage an understandable interface, few researchers have studied implementation of a platform, which combines all devices of a low-level control together. Researches have tended to focus on simulation and investigation of one device or group of similar working sensors rather then apply their knowledge to design a platform, which allows an end user, an operator or a future researcher to work with an evident and easy to work interface.

In spite of these early observations, the question remains if it is possible to develop a system combining different sensors subsystems with individual properties and features and provide people with an intuitive interface.

This question occurred during a process of development of a mobile assembly robot (Figure 2) in LUT (Lappeenranta University of Technology). In this project, it was important to make the right decision about handling different sensory subsystems such as inertial, temperature and distance sensors.

Figure 2. Design of mobile assembly robot LUT.

The ROS-operated (Robot Operating System) mobile assembly robot TIERA is a project of LUT. The main purpose of the robot is repair and assembly in hazardous and dangerous for human beings areas. As it does not work in direct contact with people, it has to be tele-operated, controlled remotely by operator from the main station.

The robot consists of some parts: a traction system, arms and grippers for fulfillment of assembly tasks, a head with a movable neck, an implemented vision system and different sensors. Environment conditions have to be monitored with a great importance as well as all sensory data has to reach the interface of the operator in that particular application.

Consequently, it was desirable to carry out surveys of lower level systems control and ways of their usage in unified interface. A research problem was to organize knowledge of theoretical principles of each device and design a platform, which considers properties, applications and data of each of them.

Hence from abovementioned question and problem, aims of the thesis are:

- Studying of the temperature, distance and inertial sensors work;
- Development of cooling system for motors, batteries and controllers inside the robot;

- Implementation of a group of distance sensors for detection obstacles;
- Analyzing of a complex IMU (Inertial Measurement Unit) system;
- Development of a robot front light control;
- Detection of all devices from the main station;
- Development of a software and interface, which combines monitoring an every device from low-level subsystems.

For accomplishing all goals different methods and algorithms were used.

First, it is worthy to mention that this thesis proposes to use LabVIEW (Laboratory Virtual Instrumentation Engineering Workbench) software to collect all data streams from sensors and control cooling system and a torch. Second, hardware presented in that project is cRIO controller made by NI Company and different devices. Connection of a main control station with devices was provided using Real-Time protocol, created by NI, and UART (Universal Asynchronous Receiver-Transmitter) protocol for IMU. Moreover, Kalman filter estimation technique was used inside IMU.

The remainder of this thesis is divided into 4 main sections. The first section is a theoretical knowledge standing behind the phenomenon of environmental conditions transformation into electrical signals. Temperature, distance and inertial sensors effects are presented. Moreover, there is information about Kalman filter method in the first part.

The main purpose of the second section is to introduce hardware and software used in experimental setup. Description of a temperature control system: thermos sensors and fans; ultrasonic distance sensors, inertial sensor is presented in that section. Furthermore, embedded controller cRIO and its connection with all devices are described. The second section also contains explanation of software used for development of a platform and presentation of an application combining data from all devices together.

The third section is aimed to show results of accomplished work and analyze them. A user interface as a final product is presented in that part. Moreover, that part contains estimation of done work and ideas for future research and improvement of the system. Finally, the last section consists of conclusion and summing up the whole thesis.

2 THEORETICAL BACKGROUND

The thesis work is based on the implementation of real devises into the existing mobile robot project. Each subsystem has individual parameters and features and for better understanding how to work with sensors and other devices it is important to know physical theory and principles of processes applied during development of a gadget. That chapter contains theoretical knowledge of construction and basis of subsystems used in the development of low-level control interface for the mobile assembly robot.

2.1 Temperature sensing effect

Temperature sensors can be classified by physical working principle to liquid (mercury thermometer), mechanical, electrical (thermocouple, resistance thermometer), optical (infrared). The most suitable type of temperature sensors for the mobile robot, which supposed to operate in hazardous area, is a resistance thermometer or RTD (Resistance Temperature Detector). There are several reasons for choosing that type of devices, which will be mentioned below. (Childs, Greenwood & Long 2000, p. 2959.)

First, resistance thermometers are very compact, that is why they can be installed easily under the cover of the robot to measure the temperature of the hottest parts. Second, the sensor uses not complicated algorithm of recounting from changeable resistance to temperature. Third, accuracy of measurement is very high for that type of sensors (usually less than ±1°C). (Edwards & Otterson 2014, p. 276.)

Abovementioned properties are provided by the usage of elaborate construction of the device. The principle of RTD work is based on a relation between electricity resistance of metals, alloys or semiconductors and temperature. The RTD consists of a resistor made from a metal wire or a film on a dielectric substrate (ceramic or glass) (Figure 3). The metal part resistance depends on the temperature. A protective overcoat covers the RTD elements, due to their fragility (Figliola & Beasley 2015).

The most prevalent and common material for the wire is a platinum, because that material has well-known and stable dependence between resistance and temperature. Moreover, platinum is not oxidized in the air, which ensures high accuracy and productivity.

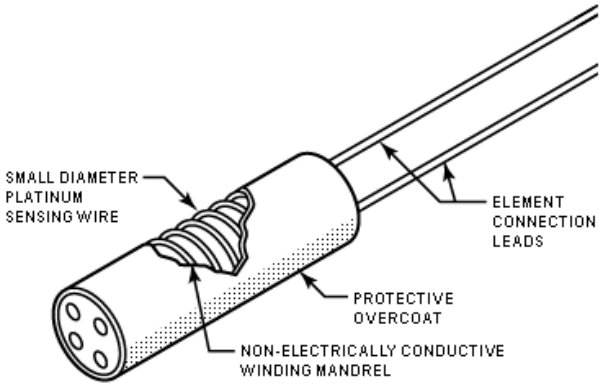

Figure 3. Construction of the resistance thermometer with a platinum wire (RdF Corporation 2003).

The most vital part of calculation of the temperature is an application of right equations, which demonstrate relationship between resistance and temperature. For platinum-based RTD equations suggested by Callendar-Van Dusen are used (IEC 60751 2008):

$$R_T = R_0\left[1 + AT + BT^2 + CT^3\left(T - 100\right)\right], -200°\mathrm{C} < T < 0°\mathrm{C}, \quad (1)$$

$$R_T = R_0\left[1 + AT + BT^2\right], 0°\mathrm{C} \le T < 850°\mathrm{C} \quad (2)$$

In equations one and 2 R_T is denoted as the resistance at the temperature $T°\mathrm{C}$, R_0 is the resistance at 0°C, and *A, B, C* are invariable coefficients, equal to:

$$A = 3.9083 \cdot 10^{-3}\ °\mathrm{C}^{-1}$$

$$B = -5.775 \cdot 10^{-7}\ °\mathrm{C}^{-2}$$

$$C = -4.183 \cdot 10^{-12}\ °\mathrm{C}^{-4}.$$

Due to relatively small values of constants *B* and *C*, the resistance grows almost linearly with the increasing temperature.

Hence, the linear approximation can be applied to resistance-temperature relationship in a range from zero to 100°C. This dependence can be characterized by coefficient:

$$\alpha_{rt} = \frac{R_{100} - R_0}{100°\text{C} \cdot R_0}, \tag{3}$$

where R_0 and R_{100} are electrical resistance at 0°C and 100°C respectively. The coefficient unit is $\Omega/(\Omega \cdot °\text{C})$ (IEC 60751 2008).

2.2 Distance estimation

Work of a distance sensor is based on analyzes of different types of waves incoming from environment. Distance sensors have a great amount of varieties depending on a theoretical physical effect, which stands behind. Ultrasound, infrared light, microwaves, radio waves et cetera can be used for distance measurement.

Another criterion of classification of distance measurement devices is a method of the work with waves. The first group of devices just generates and sends waves to the environment. Such devices are called active or transmitters. The purpose of the second group is signal receiving. The name of that group is receivers. Moreover, the last group combines both tasks: transmitting and receiving the signal and it is called transceivers. As a rule, this group of devices uses the same type of waves.

Each combination of the wave type used in a sensor has advantages and disadvantages. The material and the color of a detected object do not affect ultrasonic sensors, whereas optical sensors can show wrong result working in front of glass or fleecy surface. Detecting distance can vary from 1 m for optical to 10 m for ultrasonic sensors. However, accuracy and response speed of optical is higher in comparison with ultrasonic. However, ultrasonic sensors have valuable advantage over optical technology sensors: they are not affected by water and dust. (Keyence Corporation 2017.)

One has to pay attention that there is a possibility of usage the mobile robot in dangerous and unknown environment (water, dust) for object detection of different types of materials.

Moreover, the high limit of distance between the robot and obstacles is not available beforehand. For these reasons, implementation of ultrasound sensors in the project is preferable.

For better understanding of ultrasonic sensors, it should be explained the principle of ultrasound waves processing. The operation method of that sensor type is based on transmitting “a short burst of sound in a particular direction” (Pallàs-Areny & Webster 2001) and receiving of reflected ultrasound waves after the time *t* (Figure 4).

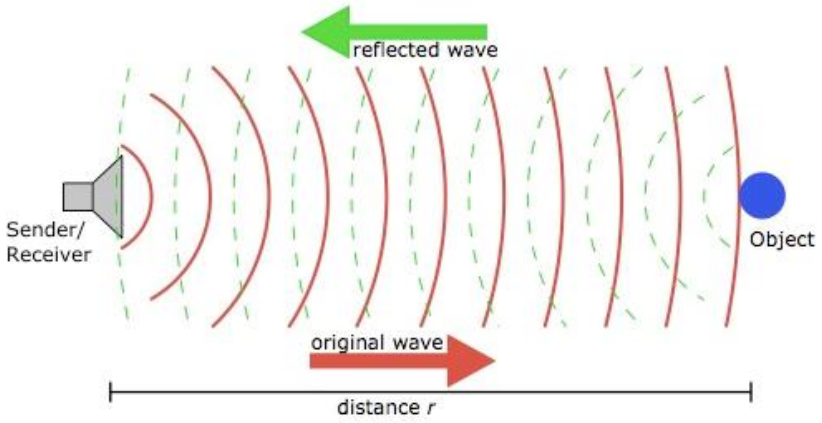

Figure 4. Logic of the transceiver operation (Pallàs-Areny & Webster 2001).

The sensor calculates the distance r_s between a sender and an obstacle based on the speed of the sound *c* (Pallàs-Areny & Webster 2001):

$$r_s = c \cdot t \tag{4}$$

According to Terzic et al. (2013, p. 11), “ultrasound waves consist of high-frequency sound waves that are inaudible to human beings” , generate changes of the air density and pressure, spreading through the space. The shape of the energy trace of a sound travelled in air is similar to the shape of sound signal, provided by a speaker. At the same time, the same effect can be applied to receivers, which get information about a sound depending on high and low pressure points. Illustration of the phenomenon is shown on a Figure 5.

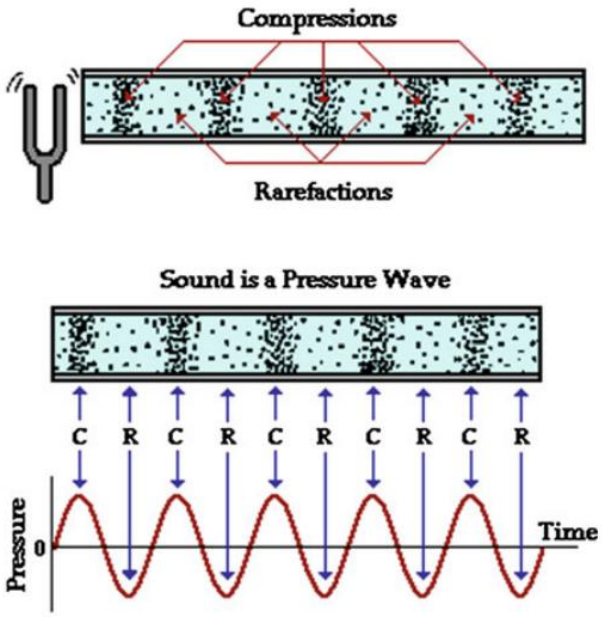

Figure 5. High and low pressure points produced by a sound of a fork (Terzic et al. 2013, p. 12).

A diaphragm of the speaker has to generate low and high pressure points by moving back and forth with the aim of producing a sound wave. In case of ultrasound, motion velocity of the diaphragm is much greater than for making audible sound. A part of the speaker moves under influence of an electrical signal. (Terzic et al. 2013.)

The diaphragm of the microphone functions oppositely. The sensitive element receives the vibration and the air pressure propagating by different parameters of sound waves. The microphone processes obtained air particles fluctuation and pressure difference and generates electrical output, which is a copy of a sound wave (Figure 6). (Terzic et al. 2013)

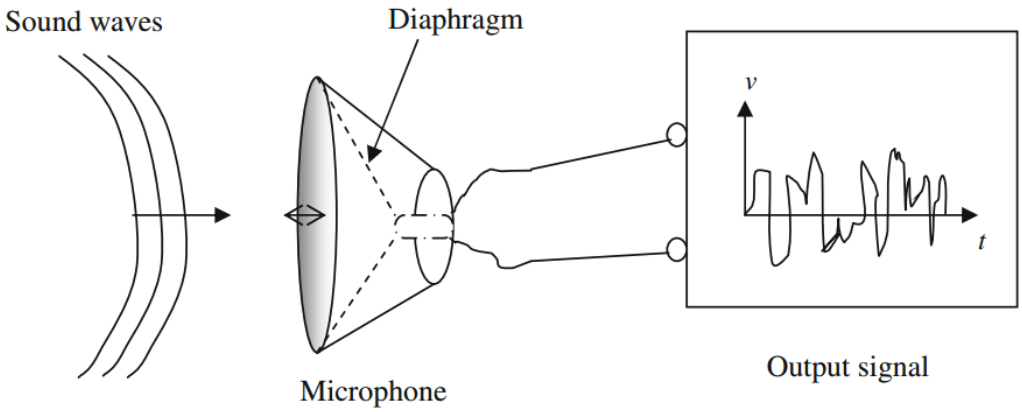

Figure 6. The principle of work of the sound receiver (Terzic et al. 2013).

The most common method of a conversion from mechanical vibration of a diaphragm to electricity signal and vice versa is a usage of piezoelectric principle of trans-conductance. A plate of the piezoelectric material possesses a property of changing its thickness depending on the electrical field occurred between metal electrodes on opposite sides of the plate.

Thereby, tuning a voltage in an electricity circuit of two electrodes one can generate expansion and compression of the piezoelectric layer and consequently produce a sound wave. That principle works in opposite direction as well: in a response to pressure difference in air particles, the material changes the dimension, which causes variable inducted voltage. (Kuttruff 2012.)

2.3 Inertial navigation system

INS (Inertial Navigation System) uses a principal of the determination of coordinates and motion parameters of variable mobile machines based on calculation of the inertia of bodies. The method is an autonomous detection of object navigation without requesting connection with outer reference points. The navigation systems based on GPS (Global Positioning System) or external satellite systems are simple for implementation, but errors can occur in case of losing connection what happens frequently.

Advantages of the INS method are:

- Possibility of autonomous work,
- Noise immunity,
- Possibility of the automation of all navigation processes.

Due to these pluses, the method is getting popular among vessels, submarines, airplanes, spaceships and other vehicles and moving objects.

Work of the INS is based on the combination of accelerometer and gyroscope data of the moving object. With their help, one can determined the deviation of the coordinate system associated with the body of the device from the coordinate system associated with the Earth. Moreover, the principle of dead reckoning is also used in navigation systems. The idea of it is the calculation of new position and orientation of the object with the reference

of previous coordinates and orientation or some initial values. New values are estimated analyzing the reference point values and time passed from the last calculation.

Thus, orientation angles: yaw (rotation of the front part to the left and right), pitch (the front part goes up and down) and roll (rotation clockwise and counter-clockwise around direction of linear motion) can be obtained. The angular deviation of coordinates in the form of latitude, longitude and altitude is determined by integrating the acceleration.

In the beginning of the method development scientists faced with a problem of necessity of consideration parameters, dimensions and masses of all devices during designing and manufacturing process. The system should be precise measurement unit. The first try to solve that problem was introduced in United States of America in 1960. The idea was to implement an accelerometer, a gyroscope and a calculation device in one machine under the same cover and call it IMU. The first prototype was as big, as it occupied almost the entire cabin of the aircraft. Since that, time technology has been improving and size of the IMU can be less than a match-box nowadays. (King 1998, p. 140-149)

Algorithmically, the IMU consists of an attitude and heading reference system and a coordinate determination system. The attitude and heading reference system provides the ability to determine the orientation in a geographical coordinate system, which allows estimating the position of the object correctly. At the same time, information about the position of the object must be sent constantly into the attitude and heading reference system. However, technically, the system, as a rule, is not divided and accelerometers can be used for the initialization of the attitude and heading reference system part.

The IMU usually includes 3 orthogonal accelerometers, 3 orthogonal gyroscopes and computer capable to process data from all devices and track the orientation and the position. Optionally, it can contain 3 magnetometers. The measured linear acceleration relates to the moving system and shows values in a body frame without understanding of an orientation of the vehicle in a space. The reason of that is installation of the sensor on the machine: not every rotation of the object is detected by accelerometer. The same situation happens with gyroscope. Since the sensor installed on a body and the available information is just about angular velocity it is not aware about linear motion. However,

combining measurements from all sensors it is possible to receive concept of the position and the orientation of the object. (Trusov 2011.)

Different construction and methods of the IMU exist. Classification of them depends on the type of sensors (gyroscope, accelerometer) and the method of their installation. IMU can include gyro-stabilizing platform or not. In case of platform devices, can gimbaled, fluid-suspended et cetera. Moreover, devices, such as strap down system, quartz rate, vibrating, ring laser, fiber optic and hemispherical resonator gyroscopes can be used for the IMU. However, the most widely used technology utilized in the IMU is a vibrating gyroscope and in particular MEMS (Micro-electromechanical Systems).

The MEMS are devices combining microelectronic and micromechanical components. Plenty of devices can be manufactured using that technology. The main aim of development MEMS is achieving of utilization of normal-size electromechanical mechanisms in the micro scale. For that purpose variety of methods, techniques and materials can be used. (Crone 2008, p. 276-282.)

The most common material for MEMS is silicon. That material possesses properties required for that application. It is easy to find, available and cheap high-quality material, which can be used for implementation in electronic circuits. Moreover, silicon mono crystal follows Hooke's law, which means that it is not subjected by hysteresis under the deformation; consequently, the most deformation energy is not dissipated. At last, that material is very reliable in high frequency motions, since it has very little fatigue and can operate in the range of billions to trillions of cycles without destruction. The main methods of obtaining all MEMS devices based on silicon are the deposition of layers of material, the structuring of these layers by means of photolithography and etching to create the desired shape.

MEMS gyroscope sensors can be divided into two groups. The first group uses an inertia measurement of the vibrating mass for receiving an angular velocity or linear acceleration (Trusov 2011). The second group uses inertial properties of oscillation waves of the resonator (Maslov, Maslov & Merkuryev 2014).

The principle of the vibrating gyro is used in a variety of applications, for example a smart phone, a photo camera or a human balancing transporter Segway. The vehicle control system consists of two microprocessors constantly calculating measurements from five vibrating gyroscopes to producing balancing properties.

The vibrating gyroscope or the Coriolis vibratory gyro is a device based on the spinning or vibrating mass (Trusov 2011). The application allows saving rotation or direction of the vibration when turning the base proportionally to angular velocity or the base rotation angle. That type of gyroscopes is much cheaper and easier for using in comparison to the rotational gyroscope with the same accuracy of the measurement.

A mechanism of the vibratory gyroscope consists of the inertial reference frame $\xi\eta\zeta$ and non-inertial frame xyz. Movement of the second in the inertial frame can be described by an angular velocity vector $\mathbf{\Omega}=\left(\Omega_x,\Omega_y,\Omega_z\right)$, where $\Omega_x,\Omega_y,\Omega_z$ denote angular velocities around *Ox*, *Oy* and *Oz* axes of the non-inertial reference frame respectively, and a linear acceleration vector $\mathbf{A_0}=\left(A_{0x},A_{0y},A_{0z}\right)$. Components of the linear acceleration vector A_{0x},A_{0y},A_{0z} mean linear acceleration in direction of *Ox*, *Oy* and *Oz* axes respectively. All abovementioned variables are given with a respect to a moving frame (**Ошибка! Источник ссылки не найден.**). Elastic forces of the suspension affect a point mass *m* in the origin of coordinates *O* of the system. At the same time, the motion of the frame xyz produces inertial which also constrain the movement of the mass in the *Oxy* plane. Thus, the mass is not under the influence of Coriolis acceleration. (Trusov 2011.)

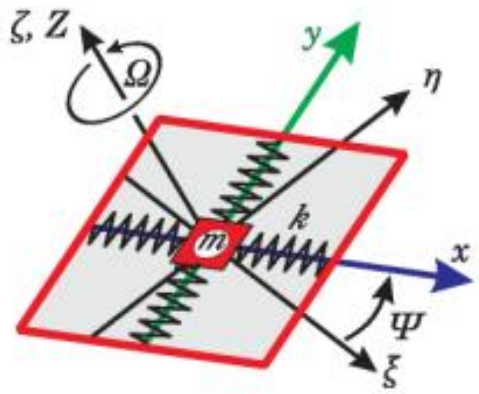

Figure 7. Model of a vibrating gyroscope (Trusov 2011).

A vector $\boldsymbol{\rho} = (\xi, \eta, \zeta)$ denotes coordinates of a mass in the inertial reference frame and a vector $\mathbf{r} = (x, y, z)$ is a mass coordinate vector in the non-inertial frame. Considering the action of a force vector $\mathbf{F} = (F_x, F_y, F_z)$, where F_x, F_y, F_z are force vector projections on axes of non-inertial reference frame *xyz*, Newton's law of the motion for the mass *m* in the inertial reference frame $\xi\eta\zeta$ is

$$\ddot{\boldsymbol{\rho}} = \frac{\mathbf{F}}{m}, \tag{5}$$

In equation 5 double dots mean the second derivative with respect to time. Position in a moving frame after differentiation is following:

$$\ddot{\mathbf{r}} = \frac{\mathbf{F}}{m} - 2[\boldsymbol{\Omega} \times \dot{\mathbf{r}}] - \left(\mathbf{A_0} + [\boldsymbol{\Omega} \times [\boldsymbol{\Omega} \times \mathbf{r}]] + [\dot{\boldsymbol{\Omega}} \times \mathbf{r}]\right). \tag{6}$$

Thus, $\ddot{\boldsymbol{\rho}}$ and $\ddot{\mathbf{r}}$ are acceleration vectors of the mass in the inertial reference frame and non-inertial reference frame respectively. The mathematical model of the Coriolis vibratory gyroscopes is presented in equation 6. Multiplication of the angular velocity vector $\boldsymbol{\Omega}$ and position vector $\mathbf{r}$ determines the connection and energy exchange between *Ox, Oy, Oz* axes. Applying vibration to the mass in the non-inertial reference frame *xyz* one can calculate angular velocity $\boldsymbol{\Omega}$ of the system. (Trusov 2011.)

Angular velocities around each axis $\Omega_x, \Omega_y, \Omega_z$ can be substitute for the vector into equation 6 as well as components of position vector $\mathbf{r}$. After opening parentheses and linearization equation 6 will be written as following system:

$$\begin{cases} \ddot{x} + x\omega_x^2 - y\dot{\Omega}_z - 2\Omega_z\dot{y} = F_x, \\ \ddot{y} + y\omega_y^2 + x\dot{\Omega}_z + 2\Omega_z\dot{x} = F_y. \end{cases} \tag{7}$$

In equation 7 ω_x and ω_y are the natural frequencies related to *Ox* and *Oy* axes, respectively. Using different modifications equation 7 can be used for two options-calculation of velocity or angle. (Trusov 2011.)

Principle of work of rate gyroscopes is division of tasks between *Ox* and *Oy* axes. *Ox* axis vibrates induced by an excitation force F_x. That process is called drive-mode. Conversely, *Oy* axis operates in the sense-mode collecting information about gyroscope rate. For rate calculation, force F_x is substituted in equation 7 by "sinusoidal waveform with amplitude *f* and angular frequency ω_d" according to Trusov (2011). After substitution, the equation 7 demonstrates open-loop mathematical model of a rate gyroscope:

$$\begin{aligned} &\ddot{x} + x\omega_x^2 - y\dot{\Omega}_z - 2\Omega_z\dot{y} = \frac{f}{m}\sin\left(\omega_d t\right), \\ &\ddot{y} + y\omega_y^2 + x\dot{\Omega}_z + 2\Omega_z\dot{x} = 0. \end{aligned} \tag{8}$$

For an ideal angle gyroscope, the system has to be symmetric unlike a rate gyroscope. An isotropic mass in the center of spring system vibrates with the same natural frequency $\omega = \omega_x = \omega_y$ for both *Ox* and *Oy* axes on a plane. External forces are not applied to the system in that case, but the inertial rotation rate Ω_z is still observed in a gyroscope with low dissipation property. Thus, mathematical model of the angle gyroscope is obtained from the equation 7 as

$$\begin{aligned} &\ddot{x} + x\omega^2 - y\dot{\Omega}_z - 2\Omega_z\dot{y} = 0, \\ &\ddot{y} + y\omega^2 + x\dot{\Omega}_z + 2\Omega_z\dot{x} = 0. \end{aligned} \tag{9}$$

This method allows the precession motion of the vibration axis in the inertial rotation space. In opposite side, rate measuring mode of the IMU demands fixed position of vibrating axis in the reference frame of the intended movement. Consequently, orientation reference for angle-mode measurement is determined instantly, as it follows inertial rotation. Besides, free vibrating axis of rate gyroscope does not have limits of mechanical motion, unlike the conventional rate-mode measuring. (Trusov 2011.)

The second group of studied MEMS gyroscope is based on oscillation wave properties. This type of gyroscopes works by usage of electrical forces applied to exert positional excitation. The gyroscope consists of thin flexible cylinder one, which maintains to the movable base 2 and a ring of control electrodes 3 around the free end of the cylinder as shown on **Ошибка! Источник ссылки не найден.**. (Maslov et al. 2014.)

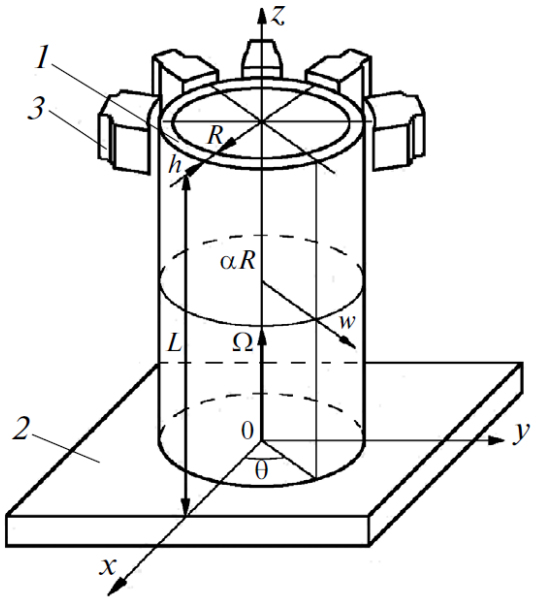

Figure 8. Model of wave solid-state gyroscope (Maslov et al. 2014).

The cylinder functions as a resonator conducting a wave excited by AC (Alternating Current) voltage from control electrodes. Furthermore, a row of coupled electrodes is installed inside the cylinder ring close to the free end. Thereby, during the wave-shape movement electrical potential between electrodes ring around the resonator and inside it is changing. Processing the changes of voltage values and comparing them with DC reference voltage information about the rotation angle can be obtained.

The main advantage of that type of gyroscope is the lack of artificially rotating parts, misalignment or fault of which can be a reason of measurement error appearance and following need of repair or replacement of device. On the other side, there is a requirement for installation of these devices on the system: angular velocity around the axis of symmetry of the cylinder has to be considerably less than characteristics of the resonator wave.

2.4 Filtering algorithms

Navigation systems such as GPS, radio stations, magnetometers (data acquisition along the course), odometers (data obtaining on the traversed path in ground application) and other satellite devices are used for compensation of accumulating errors in orientation angles and coordinates. The compilation of the data from various navigation systems is carried out according to an algorithm based on a filtering of the signal. The most common filter is Kalman filter, but for reducing noise or errors other filters can be used also. In addition, it must be mentioned that for ground vehicles or objects moving just on the Earth surface Schuler tuning has to be included in the estimation process.

The Kalman filter is a recursive algorithm calculating the state vector of a changing system using an analysis of the incomplete and noisy data determining the system. The algorithm is intended for recursively overestimating the state vector of a previously known dynamical system. The filter has to possess the information about real-time values of the system and state of the filter on a previous step for the assessment of a system current state. Thus, the Kalman filter is implemented in time rather than a frequency representation. Moreover, based on the equation of conditional probability the filter determines density of distribution of the state vector. (Siciliano & Khatib 2016.)

The algorithm works in two stages. At the prediction stage, the Kalman filter extrapolates the system state values and their densities of distribution. At the second stage, the extrapolation results are updated with the measurement data variables. (Kalman 1960, p. 35-45.)

The Kalman filter uses a probabilistic model of target dynamics that specifies the type of probable movement of an object, which allows reducing noise exposure and obtaining good estimates of the object position at the present, future, or past time. The Kalman filter operates with the principle of the system state vector, which determines the state of the system at specific time. In addition it calculates statistical description of the system state.

There are several varieties of the Kalman filter, differing in approximations and assumptions, which have to be applied to making the described filter type and reduce its dimension:

- Extended Kalman filter is based on reduction of non-linear observations models by means of linearization by Taylor series expansion;
- Unscented Kalman filter is used in cases where simple linearization leads to the destruction of useful links between the components of the state vector. In this case, the "linearization" is based on the unscented transform;
- Ensemble Kalman filter is used to reduce the dimension of the task;
- Variants with a nonlinear additional filter allow non-Gaussian observations to be normal;
- Variants with a "whitening" filter allow working with "color" noises and et cetera.

Kalman filters split linear dynamic systems into discrete samples. Markov chains using linear operators and terms with normal distribution model such systems. A vector of finite dimension, the state vector, describes the state of the system. In each clock cycle, a linear operator acts on the state vector and transfers it to another state vector (deterministic state change), a certain vector of normal noise (random factors) is added and in general a control vector modeling the effect of the control system.

The Kalman is similar to hidden Markov models, with the distinction that the variables describing the state of the system are elements of an infinite set of real numbers (in contrast to a finite set of state space in hidden Markov models). In addition, the hidden Markov models can use arbitrary distributions for subsequent values of the state vector, in contrast to the Kalman filter using the model of normally distributed noise. There is a strict relationship between the Kalman filter equations and the hidden Markov model.

When using the Kalman filter to obtain estimates of the process state vector from a series of noisy measurements, it is necessary to present the model of this process in accordance with the filter structure in the form of a matrix equation of a certain type. For each clock cycle *k* of the filter operation, it is necessary, in accordance with the description below, to determine the matrices: the state-transition matrix $\mathbf{F}_k$; the observation matrix $\mathbf{H}_k$; the covariance of the process noise matrix $\mathbf{Q}_k$; covariance of observation noise matrix $\mathbf{R}_k$; in the presence of control actions, the matrix of their coefficients $\mathbf{B}_k$.

The system model implies that the true state at the moment *k* is obtained from the true state at time *k-1* in accordance with the equation:

$$\mathbf{x}_k = \mathbf{F}_k \mathbf{x}_{k-1} + \mathbf{B}_k \mathbf{u}_k + \mathbf{w}_k, \tag{10}$$

where vector $\mathbf{x}_{k-1}$ is a state vector at the moment *k*-1; $\mathbf{B}_k$ is the control matrix; $\mathbf{u}_k$ is the control vector; $\mathbf{w}_k$ is a normal random process with zero mean of distribution *N* and the covariance matrix $\mathbf{Q}_k$ describing the random evolution of the system as

$$\mathbf{w}_k \sim N(0, \mathbf{Q}_k). \tag{11}$$

At the moment *k*, there is an observation vector $\mathbf{z}_k$ of the true state vector $\mathbf{x}_k$, which are related to each other by the equation:

$$\mathbf{z}_k = \mathbf{H}_k \mathbf{x}_k + \mathbf{v}_k, \tag{12}$$

where $\mathbf{H}_k$ is the measurement matrix connecting the true state vector and the vector of measurements made, $\mathbf{v}_k$ is the Gaussian white noise with zero mean of distribution and the covariance matrix $\mathbf{R}_k$:

$$\mathbf{v}_k \sim N(0, \mathbf{R}_k). \tag{13}$$

The initial state and vectors of random processes on each cycle $\{\mathbf{x}_0, \mathbf{w}_1, ..., \mathbf{w}_k, \mathbf{v}_1, ..., \mathbf{v}_k\}$ are considered independent.

To calculate the evaluation of the state of the system for the current cycle of work, it needs an assessment of the state (in the form of an assessment of the state of the system and an estimate of the error in determining this state) on the previous operating cycle and measurement at the current clock cycle. This property distinguishes it from packet filters

that require knowledge of the history of measurements and/or estimates in the current cycle of operation.

Value $\hat{\mathbf{x}}_{n|m}$ is denoted as an estimation of the true vector **x** at the moment *n* taking into account the measurements from the moment of starting work and at the moment *m* inclusive. The filter state is specified by two variables. The first of them $\hat{\mathbf{x}}_{k|k}$ is a posteriori estimation of the state of the object at the moment *k* obtained from the results of observations up to the moment *k* inclusive. The second variable $\mathbf{P}_{k|k}$ is a posteriori error covariance matrix specifying an estimate of the accuracy of the obtained state vector estimate. In addition, the second variable includes an estimate of the variance of the calculated state and covariance showing the revealed relationships between the system state parameters.

Each iteration of the Kalman filter is divided into two phases: prediction and update. During predictions, the filter receives a preliminary estimate of the state of the system $\hat{\mathbf{x}}_{k|k}$. This preliminary estimate is also called an a priori estimate of the state, since the observations of the corresponding step are not used to obtain it. The update stage is the merge of a priori prediction and corresponding current measurements with the aim to correct the estimate. The corrected estimate is also called a posteriori state estimate, or an estimate of the state vector $\hat{\mathbf{x}}_k$.

Usually these two phases alternate: the prediction is made according to the correction results until the next observation, and the update is made in conjunction with the observations available at the next step et cetera. However, if the observation was not available, the update stage may be skipped and predicted from an uncorrected estimate. Likewise, if independent measurements are only available in separate work cycles, updates are still possible (usually using a different observation matrix $\mathbf{H}_k$).

Extended Kalman filter stages will be discussed. Prediction of the state vector of the system by estimating the state vector and the applied control vector from step (*k*-1) to step *k* is

$$\hat{\mathbf{x}}_{k|k-1} = f\left(\hat{\mathbf{x}}_{k-1|k-1}, \mathbf{u}_{k-1}\right). \quad (14)$$

In equation 14 $f(.)$ denotes a function of transition, $\hat{\mathbf{x}}_{k-1|k-1}$ is an estimation of the state of the object at the moment *k*-1 obtained from the results of observations up to the moment *k*-1 inclusive, $\mathbf{u}_{k-1}$ is the control vector at the moment *k*-1.

Covariance matrix for the predicted state vector:

$$\mathbf{P}_{k|k-1} = \mathbf{F}_{k-1}\mathbf{P}_{k-1|k-1}\mathbf{F}_{k-1}^{T} + \mathbf{Q}_{k-1}, \quad (15)$$

where $\mathbf{P}_{k-1|k-1}$ is a posteriori error covariance matrix, $\mathbf{Q}_{k-1}$ is a covariance of the process noise matrix and $\mathbf{F}_{k-1}$ is a transition matrix for the moment *k*-1.

On update step following values are estimated. The deviation of the observation obtained at step k from the observation expected during prediction stage:

$$\tilde{\mathbf{y}}_k = \mathbf{z}_k - h\left(\hat{\mathbf{x}}_{k|k-1}\right), \quad (16)$$

where $h(.)$ is an observation function.

Covariance matrix for the deviation vector (error vector):

$$\mathbf{S}_k = \mathbf{H}_k\mathbf{P}_{k|k-1}\mathbf{H}_k^{T} + \mathbf{R}_k. \quad (17)$$

The Kalman optimal matrix of gain factors, formed based on covariance matrices of the available prediction of the state vector and the obtained measurements (through the covariance matrix of the deviation vector):

$$\mathbf{K}_k = \mathbf{P}_{k|k-1}\mathbf{H}_k^{T}\mathbf{S}_k^{-1}. \quad (18)$$

Update of the previously obtained extrapolation of the state vector - obtaining an estimate of the state vector of the system:

$$\hat{\mathbf{x}}_{k|k} = \hat{\mathbf{x}}_{k|k-1} + \mathbf{K}_k \tilde{\mathbf{y}}_k . \tag{19}$$

Calculation of the covariance matrix for estimating the state vector of the system:

$$\mathbf{P}_{k|k} = \left(\mathbf{I} - \mathbf{K}_k \mathbf{H}_k\right) \mathbf{P}_{k|k-1}, \tag{20}$$

where, $\mathbf{I}$ is an identity matrix. Besides, state transition and observation matrices will be Jacobian matrices, denoted by

$$\begin{aligned} \mathbf{F}_{k-1} &= \left.\frac{\partial f}{\partial \mathbf{x}}\right|_{\hat{\mathbf{x}}_{k-1|k-1}, \mathbf{u}_{k-1}}, \\ \mathbf{H}_k &= \left.\frac{\partial h}{\partial \mathbf{x}}\right|_{\hat{\mathbf{x}}_{k-1}} . \end{aligned} \tag{21}$$

The extended Kalman filter is a universal tool for elimination of accumulating error from different types of devices. For example, the gyroscope and the accelerometer used in that work suffer from progressing deviation from the real values due to integration and derivation errors. In that case, usage of filtering algorithms is necessary for accurate work of the system.

3 EXPERIMENTAL SETUP

The main part of the project is based on the programming real devices for the robotic system. Implementation of sensors and indicators on the mobile assembly robot was the priority of the thesis work. As it was mentioned before, each device has its own structure and principle of work. Combination of different types of electrical and logical connections is used for provision of the decent work of all gadgets.

This chapter is designated to provide information about specific properties of used devices, their working conditions and connection protocols. Besides hardware description, software utilized in the project is introduced. Moreover, the chapter includes explanation of the designed program code implemented to the control system of the robot.

3.1 Temperature control system

Inner parts of the robot such as main computer, drivers, motors, additional controllers and a battery are subjected to heating due to their working process. Moreover, all devices are installed under the cover of the mobile robot, which means they do not have air circulation. The temperature control system was implemented to the project to avoid overheating of the system and possible failure.

The temperature control system consists of two temperature sensors and three fans. Temperature sensors are installed close to the most influenced by heat parts. Two fans are placed on the front panel of the robot cover to suck in air from the outside and another fan is mounted on the back part of the robot to blow out hot air from the internal space of the robot. Logic of their collaboration will be explained further in software description section.

For temperature measurement, the sensor made by MINCO Company was chosen. A model S102408PD3G40 is shown on a Figure 9. The temperature sensor is a compact, compatible with different controllers and easy for installation. The RTD element of the sensor is presented by platinum wire. Main features of the particular temperature sensor are demonstrated in a table 1.

Figure 9. Temperature sensor MINCO (Minco Components 2015).

Table 1. Properties of the temperature sensor Minco S102408PD3G40 (mod. Minco Components 2015).

Property of the device	**Value or characteristic**
Dimensions	∅ 4.8×60.5 mm
Element type	Platinum
Case material	Stainless steel
Temperature range	-70 to 550 °C
Resistance	$100\,\Omega \pm 0.12\%$ at 0°C
Resistance-temperature coefficient	$0.00385\ \Omega/(\Omega\cdot°\mathrm{C})$
Vibration range	10 to 2000 Hz

Fans utilized in the temperature sensor system are made by SUNON Company. The model used in the project DC brushless fan PMD2412PMB1-A is shown on a Figure 10. Specification of the device is summarized in a table 2. Construction of the fan allows installing it in any direction considering that air flows toward the label side direction. According to a fan datasheet, it is necessary to power it with voltage more than 10 V to make it run. Thus, the analog fan control through changes of DC voltage value can be replaced with digital control and logical zero and one for turning on and off the fan.

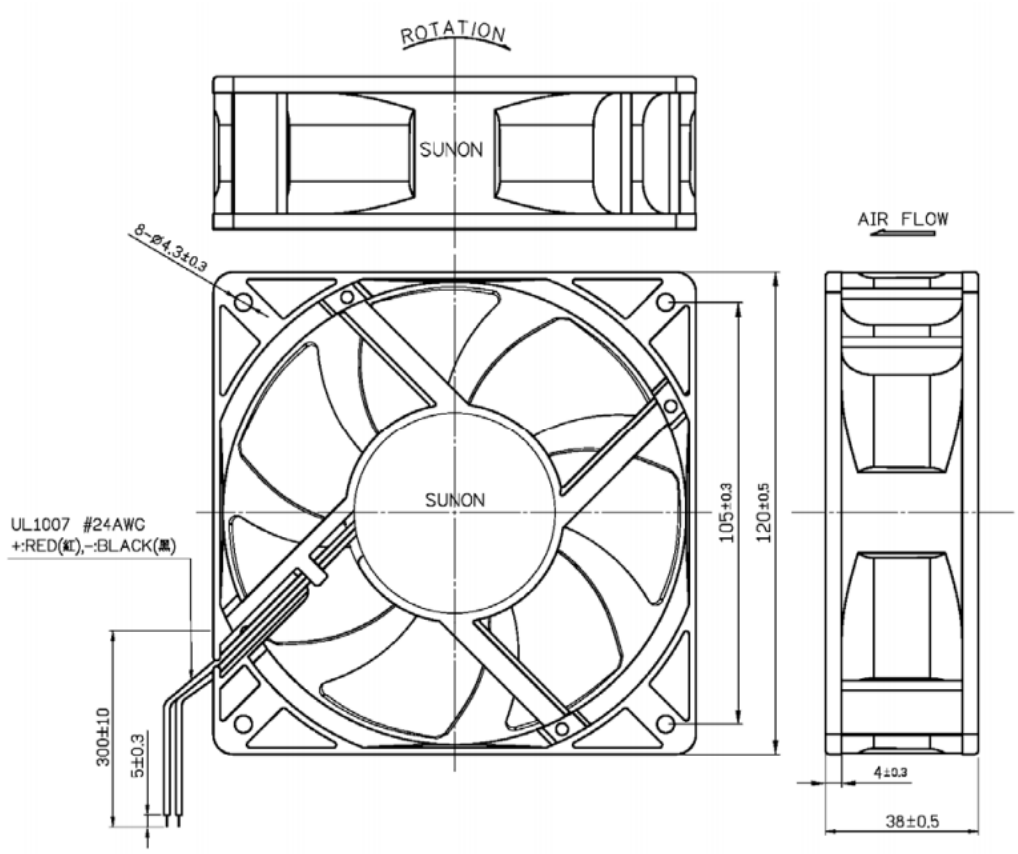

Figure 10. SUNON PMD2412PMB1-A fan (SunonWealth Electric Machine Industry Co. 2014).

Table 2. Properties of the fan SUNON PMD2412PMB1-A (mod. SunonWealth Electric Machine Industry Co. 2014).

Property of the device	**Value or characteristic**
Dimensions	120×120×38 mm
Rated voltage	24 V
Operating voltage range	10-27.6 V
Starting voltage	10 V
Rated speed	4200 ±10% RPM (Revolutions Per Minute)
Air delivery	0.0566337 m^3/s
Rated current	760 mA
Rated power	18.2 W
Noise level	54 dB
Operating temperature	-10 to 70 °C

3.2 System of distance monitoring

The object detection is very important task for the mobile robot. All sides of the robot are equipped with distance sensors: two units are mounted on each side to cover whole area around the robot. The used ultrasonic sensors model SRF06 is shown on a **Figure 11**. The technical data of that device is introduced in the table 3.

Figure 11. Ultrasonic distance sensor SRF06 (Manu Systems AG 2017).

Table 3. Properties of the Ultrasonic distance sensor SRF06 (mod. Manu Systems AG 2017).

Property of the device	**Value**
Dimensions	43×20 mm
Distance range	0.02-5.1 m
Current output	4-20 mA
Current power loop	4-20 mA
Nominal current	4 mA+31.37 µA/cm
Loop driving voltage	9-24 V
Period of ranging	70-100 ms
Frequency	40 kHz

According to table 3, current output values do not represent real distance measurement. Translation between output signal and required distance value is realized programmatically as well as filtering from noise, disturbances and over limits values.

3.3 Functionality and description of inertial sensor

The inertial sensor 3DM-GQ4-45 (Figure 12) by LORD MicroStrain Company implemented to the project has many functions. Basically, it is an inertial navigation system combines in a compact shape MEMS accelerometer and gyroscope, magnetometer, pressure altimeter, GNSS (Global Navigation Satellite System) and processor for filtering data (Extended Kalman filter) and computing of different characteristics (roll, pitch, yaw angles, orientation matrix, delta velocity vector, quaternion) from available ones. Moreover, the device includes algorithms for magnetic, temperature and linear acceleration compensation.

Figure 12. Inertial sensor (LORD MicroStrain 2016).

Main properties of the INS are provided in a table 4. It has to be indicated that the physical unit for accelerometer measurements is g such as 1 g = 9.80665 m/s^2. All values received by sensor are subjected to post processing and filtering. The sequence of the filtering is following, according to LORD MicroStrain (2016):

- "Analog bandwidth filter";
- "Digital sigma-delta wide band anti-aliasing filter";
- "Digital averaging filter sampled at 8 kHz and scaled into physical units";
- "Coning and sculling integrals computed at 1 kHz".

Besides, extended Kalman filter is implemented into the computing software of the inertial system. By virtue of the complex filtering system, accuracy of the device is estimated as

±0.1 m/s for velocity measurements and two decimal places for acceleration and angular velocity.

Table 4. Specification of the 3DM-GQ4-45 inertial sensor (mod. LORD MicroStrain 2016).

Property of the device	**Value**		
	Accelerometer	**Gyroscope**	**Pressure Altimeter**
Measurement range	±5g	300°/s	-1800 to 10000 m
Resolution	<0.04 mg	<0.0025°/s	<0.1 m
Sampling rate	10kHz	10kHz	25 Hz
IMU data output rate	1-500 Hz		
Computed data output rate	1-500 Hz		
Power source	4.2-28 V DC		
Power consumption	2.5 W		
Operating temperature	40-85 °C		
Dimensions	76.2×65.4×18.9 mm		

The sensor can be connected to the computer or controller by means of two methods. The first possibility is the usage of USB 2.0 (Universal Serial Bus) protocol of data transmission. Another approach of handling connection between the INS to computer is the RS232 (Recommended Standard 232) port or UART serial interface usage. In case of the first, there is no need in additional power source, but in case of serial connection DC voltage source mentioned in the table 4 has to be applied.

There is an important difference between USB and UART. Even though USB connection generates virtual serial port, logic of their work is not similar (LORD MicroStrain 2015). USB protocol connection uses master-slave system: computer (master) opens connection and polls sensor (slave). The disadvantage of the master-slave protocol is data drops caused by latency; the slave can send information to the master just after receiving request. Thus, sensor data arrives to user inconstantly; some information can be lost between the polling moment and the moment of reply. UART protocol does not provide master-slave,

but allows receiving streaming data from the device. That is why it is preferably to implement INS with serial connection into the project.

Developers of the inertial sensor provide consumers with ready-to-use software, but it is not suitable for implementation into the united low-level subsystems program. That was a reason to prefer serial connection coding and to work with sets of hexadecimal numbers of commands and data. Logic of work with INS will be explained further.

3.4 Embedded system cRIO and input/output modules

All lower level subsystem devices have different configurations and connection features. Merger of every sensor data and every control signal is executed by controller NI cRIO model 9035 (Figure 13) with C (compact) Series modules which can be installed on empty slots of the controller. One more advantage is that they can be reconfigurable or removed fast and easy which makes system very flexible to changes.

Figure 13. CompactRIO-9035 controller (National Instruments 2017a).

The model is equipped with the Real-time processor Intel Atom and FPGA Kintex-7, which are designed to work with streaming data, controlling and monitoring of connected devices. Variety of ports on the controller allows getting access to devices mentioned before. Ports include two USB 2.0 (standard size), a USB 2.0 (mini), two serial ports with different configurations, and 8 slots for C series modules. Besides, it has mini display port and slot for SD (Secure Digital) card. (National Instrument 2016a.)

Furthermore, cRIO-9035 can be connected to computer by means of Ethernet cable or using USB. In terms of reliability, the first option is more preferable. In that particular case

(the mobile assembly robot project), it is connected to the main control station indirectly but through a router. There is a physical Ethernet link between controller and the router, both mounted on the robot. Further the router transmit/receive signal to/from main station by Wi-Fi (Wireless Fidelity) protocol.

Major parameters of the cRIO-9035 controller are indicated in a table 5. According to them, one can conclude that embedded input-output system is very powerful and fast. That is why controller requires power supply to run processor and transmit this electricity further to C Series modules. Most of them do not need additional power source besides amount of energy they receive from the controller plugging into it. Nevertheless, there are some modules specifying demanding supplementary power supply for correct work.

Table 5. Specification of NI cRIO-9035 embedded system (mod. National Instrument 2016a).

Property of the device	**Value or characteristic**
Dimensions	328.8×88.1×109.2 mm
CPU (Central Processing Unit)	Intel Atom E3825
CPU frequency	1.33 GHz
Supported operating system	NI Linux Real-Time (64-bit)
Processor memory	1 GB
FPGA type	Xilinx Kintex-7 7K70T
Voltage input range	9-30 V
Maximum power consumption	46 W
Recommended power supply	100 W, 24 V DC
Operating temperature	-20 to 55°C

Variety of C Series modules allows developing the desirable system for monitoring temperature sensors data, ultrasonic distance sensors information, controlling fans and light and executing communication between computer and the INS. In following paragraphs there will be described which modules were used for connection with low level devises.

The NI 9217 (Figure 14), is an analog input module designed to transform the voltage signal from temperature sensors into understandable temperature value in °C using ADC

(Analog to Digital Converter). Properties and requirements for installation of the module are given in a table 6. It is worthy to mention that some values are valid just for 3 wire RTD, utilized temperature sensor MINCO can be included in that category.

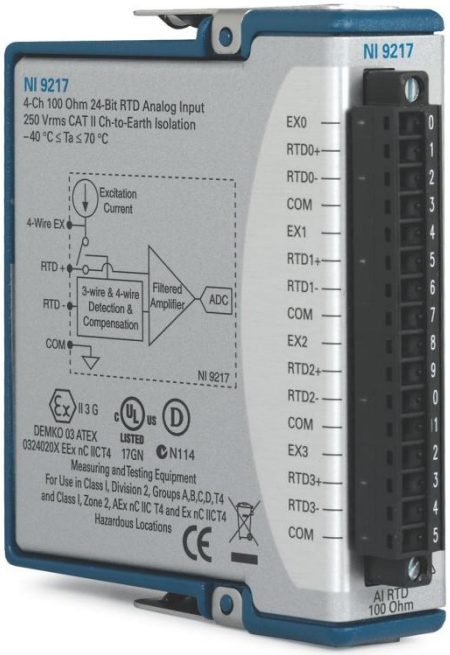

Figure 14. C Series temperature input module (National Instruments 2017d).

Table 6. Specification of NI 9217 analog input module (mod. National Instrument 2016b).

Property of the device	**Value or characteristic**
Input resistance range	0-400 Ω
Number of input channels	4
Maximum sample rate	400 S/s
Operating temperature range	-40 to 70 °C
ADC resolution	24 bits
Sampling mode	Scanned
Measurement temperature range	-200 to 850°C
Conversion time (high-resolution mode)	200 ms per channel
Conversion time (high-speed mode)	2.5 ms per channel
Temperature accuracy	0.2 °C
Maximum power consumption from chassis	350 mW
Excitation current per channel	1 mA

Temperature sensors based on resistance-temperature relation can be produced in modifications with three or four input wires. NI 9217 determines what processing algorithm has to be used depending on quantity of wires. Moreover, it calculates values according to resistance-temperature relation of platinum RTD. Logic of the work of that module is demonstrated on a **Figure 15**. Input circuit of NI 9217 (National Instrument 2016b).**Figure 15**.

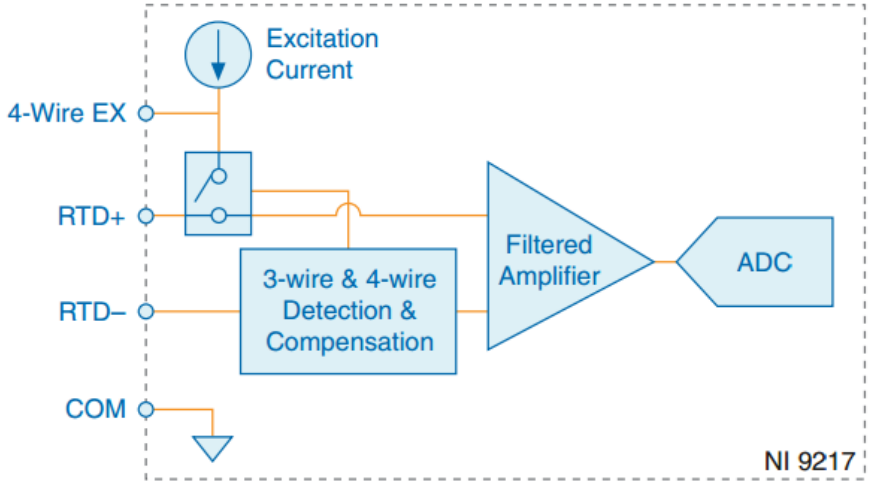

Figure 15. Input circuit of NI 9217 (National Instrument 2016b).

Three or four wires from temperature sensor are connected to the module. NI 9217 detects amount of wires and collect voltage from all of them. Then filtering of signals and amplification occur. After obtaining pure and strong analog signal, ADC generates digital signal which demonstrates temperature changes in °C units.

The NI 9203 (**Figure 16**) is a C Series current analog input module designed for collecting analog input information and processing it into discrete signal for computer (National Instrument 2014). The module is necessary to implement in the project for work with distance sensors. An output signal from them is the current measurement, increase or decrease of it describes distance to the object in space.

When the sensor and the module are connected, analog current signal is transformed into digital signal by dint of the ADC. Further, the digital signal can be translated into distance data programmatically. Properties and conditions of the module work are presented in a table 7.

Figure 16. C Series current input module (National Instrument 2017b).

Table 7. Specification of NI 9203 analog input module (mod. National Instrument 2014).

Property of the device	**Value**
Input current range	0-20 mA
Number of input channels	8
Maximum sample rate	192 kS/s
Operating temperature range	-40 to 70 °C
ADC resolution	16 bits
Calibrated gain error	±0.04%
Maximum power consumption from chassis	399 mW
Excitation current per channel	1 mA

Besides input modules for work with sensors, output modules for fans and light control have to be implemented. The NI 9472 (**Figure 17**) is a digital output module (National Instrument 2016c). Properties of it are provided in a table 8. The module can be connected with 8 devices for realization discrete logical control: TRUE and FALSE. It is certain that the module is suitable for turning on and off devices such as fans and a light.

Figure 17. C Series digital output module (National Instrument 2017c).

Table 8. Specification of NI 9472 digital output module (mod. National Instrument 2016c).

Property of the device	**Value or characteristic**
External power supply voltage (V_{sup}) range	6-30 V DC
Number of output channels	8
Typical output impedance (R_{out})	0.07 Ω
Maximum output impedance	0.13 Ω
Continuous output current (I_0)	0.75 A
I/O (Input/Output) voltage protection	30 V DC
Operating temperature range	-40 to 70 °C
Maximum output delay	100 µs
Maximum power consumption from chassis	230 mW

Operation process of the module can be explained analyzing circuit on a **Figure 18**. A device is connected to the module and to the external power supply. Current necessary for the supply of the device goes inside the module where the switcher controlled by the discrete signal opens or closes an electricity gate for the device turning ON or OFF. Output voltage from the module is calculated as

$$V_0 = V_{sup} - \left(I_0 \cdot R_{out} \right). \tag{22}$$

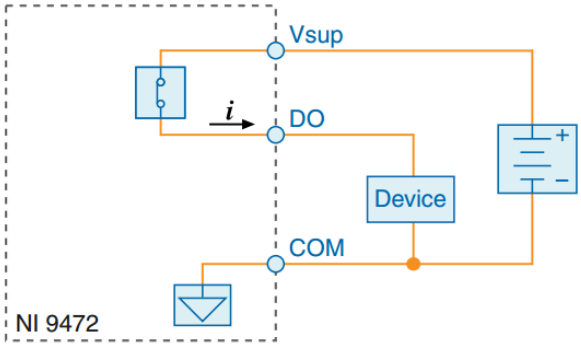

Figure 18. NI 9472 module circuit (National Instrument 2016).

Serial communication between the controller and the INS can be organized through two approaches. The first one is the usage of the serial port RS232 on the cRIO-9035 itself. The second option is the implementation of the C Series module NI 9870 (**Figure 19**) which also contains RS232 ports.

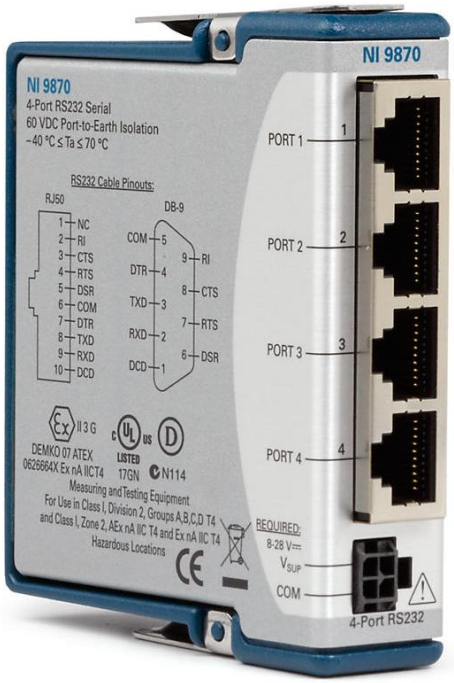

Figure 19. C Series serial instrument control module (National Instrument 2017).

However, in both cases the modification of the RS232 in NI devices is not standard, thus, it is necessary to use an adapter from NI modified serial port to RS232 cable from the LORD MicroStrain inertial system.

3.5 Software review

The software used for the project connects all devices together in one program launched on the main control station. There are some levels of software system organization. Firstly, it is necessary to find the cRIO controller mounted on the robot. The NI MAX (Measurement & Automation Explorer) software allows getting access to embedded system by means of searching IP (Internet Protocol) address of the device and setting a communication protocol between it and application from the computer.

The cRIO-9035 has static IP address with the aim of receiving the easiest and fastest access to the device. The found system provides the NI MAX with a list of its properties, which can be changed in the same program window. Moreover, all settings and drivers installation for the cRIO-9035 are executed in the same program environment. In addition, it is possible to open and modify NI Linux Real-Time operating system content through the NI MAX.

Secondly, the main application for the system is designed in the LabVIEW program. The software offers instruments for creation a project with the real-time embedded system. All data from C Series modules can be added to the project and utilized in the code as controls or indicators depending if they are input or output signals. Each program called VI (Virtual Instrument) consists of front panel (user interface) and back panel with the code. The code is written on a graphical language G that contains abovementioned control and indicator blocks as well as function and subroutine called subVI.

The LabVIEW includes a plenty of libraries, but for that work Programming, Real-Time, Data communication and Serial libraries were used. All libraries are focused on operation with their own data types flows. Some of them are standard such as double, float, string, but other designed for specific tasks, for example, accomplishment of data transition and receiving through the serial port.

3.6 Connection with the TIERA robot

The mobile assembly robot TIERA is a complicated system with many different sections: traction part, arms, grippers, head, vision system and low-level sensor system. Most of them are connected to an onboard computer, which sends and receives signals through Wi-Fi communication between the robot and the main control station. A local net allows to produce control messages for movement of robot sections, which are published into ROS topics by the main station. Then onboard computer subscribes to topics and reads messages. From the computer installed on the robot a signal spreads to each device according to instructions.

The traction section is presented by four Mecanum wheels demonstrating rotation and motion of the robot in any direction without necessity of additional mechanisms installation. Wheels are controlled by the computer Advantech, which is connected to the main station with an operator. The operator has a manipulator for control of wheels rotation speed, direction and torque. Signals from a remote control reach the main station, and then they are processed in ROS and sent to the Advantech by Wi-Fi. The Advantech is connected directly to the wheels' driver by serial port communication protocol. Thus, wheels establish assigned task.

The robot is equipped with two arms designed by Universal Robots Company. Each of them has six degrees of freedom and their own Ethernet communication protocol addresses. Arms control is realized with haptic technology devices repeating six rotational joints of arms. Position and orientation of the joystick end effector is used for computation of rotational angles of each joint of the robot arm. Direct and forward kinematics is calculated in ROS on the main station and generalized coordinates for arms control reach controllers inside mechanisms. The result of the arm work is obtaining of scaled position values and orientation values from haptic controllers.

Grippers from Robotiq Company are mounted as end effectors on arms for carrying objects and holding tools. They are controlled by haptics as well as robotic arms. Three fingers of the gripper can be closed or open depending on command from the button on the controller. In addition, haptic device produce feeling of holding or carrying an object. The

haptic or kinesthetic feedback technology realizes load sense modeling for operator work improvement.

Moreover, the TIERA robot is equipped with vision system: two cameras are installed on both arms, in a close distance to grippers and two other cameras work inside the rotating head. Information from cameras is transmitted to the main station through Wi-Fi. The special device for real-time image processing divides all video signals into two streams.

The first stream is a video signal from two cameras on arms. That video is translated on two monitors on the control station. Another stream from two cameras in the head can be shown as three-dimensional image on a big screen or post processed in a LabVIEW program for image acquisition and pattern recognition. The robot is able to recognize signs or posters warning of danger.

As it was explained before robot sections operate under control of ROS and some of them have application in LabVIEW program software. It is possible to merge code from each part together into the one control program, which is responsible for monitor and control of every device of the robot. Controllers of those devices are placed into the one local network, which allows to get communication between all of them.

The cRIO controller and all low-level devices can be integrated into the whole robotic system using LabVIEW library for publishing information into ROS topics in the same local net. The LabVIEW application runs on the cRIO and on the main station at the same time. The user interface translates information from sensors and the same information after publishing into topics can be used at the same time for other sections of robot. For example, wheels must be stopped if distance to an obstacle is less than critical.

The ROS and LabVIEW collaboration allows usage of different types of devices and controllers connected to the one network. Organization of the system in the same network is necessary for design of the united system of various groups of hardware and software.

3.7 Application description

The whole code can be divided into logical parts. Each of the parts is responsible for work with different sensors or system of devices such as temperature control system. Different parts of the code can work simultaneously or they can be turned on and off according to request of the operator. By default, all parts of the code demonstrate sensors data and condition of other devices together.

The first logical part of the program is the temperature control system, which works according to an algorithm shown on a **Figure 20**. The temperature from the robot reaches the controller, then faces comparison with the critical value and follows two scenarios: repetition of measurement reading or turning on cooling devices and then going to the start of the cycle. The whole section is placed inside while-loop, which ends as soon as Stop button is pressed.

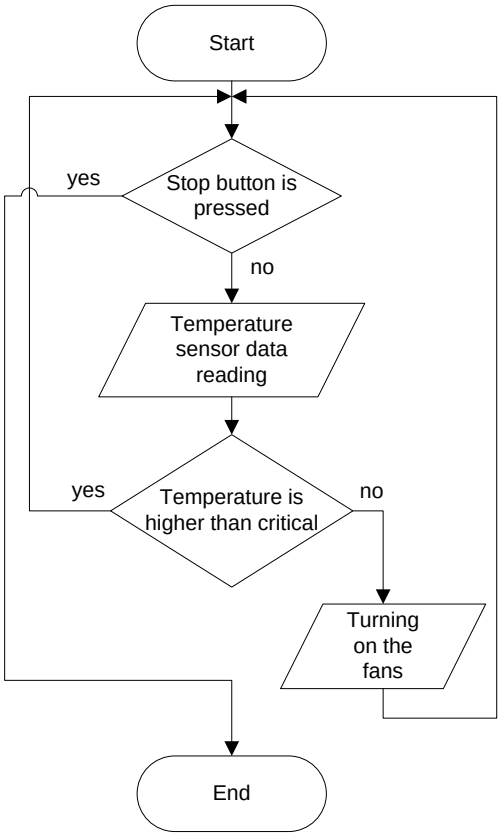

Figure 20. Algorithm of the temperature control system work.

The second section of the program is the distance-monitoring interface. Information from all ultrasonic sensors is implemented to the code as control blocks. As it was mentioned before, distance sensors send current measurement to the C Series module, which

transforms an analog signal to digital one. However, that data does not demonstrate distance in meters. For translation of current data into meters, relation between current and the distance to an obstacle is applied.

After translation process, filtration is applied to the signal. Noise and disturbances are eliminated by the usage of comparison between series of measurements. It is assumed that difference between two coherent signals cannot be bigger than some limit values. That is why there is a bandwidth-reducing amount of noise for each current measurement.

All 8 ultrasonic sensors are organized in the system to be utilized in the critical distances program interface. Every sensor signal goes through three stages of assessment depending on a distance value between the sensors and as sequence the robot and obstacle or wall. There are three critical zones around the mobile robot: the red zone is the closest to the robot (0-20 cm), the orange zone is a moderate danger (20-40 cm) and the yellow zone is the safest from all critical zones (40-60 cm). When the measurement gets into one of these limits, the interface of the program informs the user about it with turning on the diode with specified color and indicating a place around the robot where the dangerous nearness occurred.

There is also small but necessary part in the developed code: the front light control. In case of the ill-lighted environment a lamp installed on the chest of the robot can be turned on by means of usage the same program. The lamp is connected to the C Series digital output module on the cRIO controller. Thus, there is an access to control switching of the light with discrete values in the LabVIEW platform.

Finally, the biggest section of the developed LabVIEW platform is the inertial sensor communication part. As it was stated before, INS is a complex device with numerous properties and features. A serial connection between the controller and the sensor was established to get access to all functions of the INS. A communication protocol uses transference of hexadecimal messages or packets between the control system and the sensor.

There are various types of packets: commands, replies and data. Commands are sent from the controller, replies are the responses from the device to the user and data can be received in controller as a stream from the sensor. The data flow is shown on a **Figure 21**. There are three sets of data: IMU, GNSS and Estimation filter and there is an individual data packet for every data set.

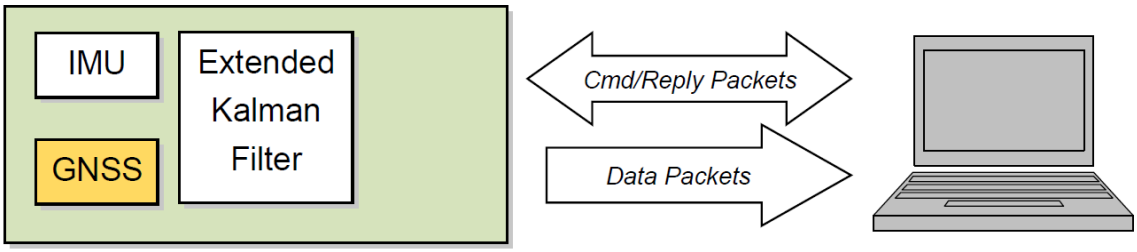

Figure 21. Communication data flow between the inertial sensor and the computer (LORD MicroStrain 2015).

The structure of the packets is the same for all types and difference of the packets is expressed just by different values of some fields. Example of the packet organization is presented on a **Figure 22**.

Header				Packet Payload			Checksum	
SYNC1 "u"	*SYNC2 "e"*	*Descriptor Set byte*	*Payload Length byte*	*Field Length byte*	*Field Descriptor byte*	*Field Data*	*MSB*	*LSB*
0x75	**0x65**	**0x01**	**0x02**	**0x02**	**0x01**	*N/A*	**0xE0**	**0xC6**

Figure 22. Packet of "Ping" command (LORD MicroStrain 2015).

The first two bytes 0x75 and 0x65 (Zero-x means representation in hexadecimal number notation) are the same for each packet and they indicate beginning of the message. The descriptor set byte determines from which set this command, reply or data is. The payload length byte is a number of bytes written in a payload section (Field Length, Field Descriptor and Field Data bytes on a figure 22).

The Field length byte is a number of bytes in one field of payload including itself. It has to be mentioned that packet payload can consist of more than one field; hence, in that case payload length and field length are not equal. The field descriptor byte is a number of a

certain command, reply or data. The field data is a set of bytes distinctive for each type of packets.

Commands do not have the field data in most cases, but if they are supposed to set new configuration or send request to get information about actual state of the device, the field data contain additional bytes about the aim of the command. Reply messages data field usually consist of command echo code, which is the repetition of the sent command descriptor byte, and error code. Meaning of the error code is ACK (Acknowledge) in case of 0x00 value and NACK (Negative Acknowledge) in case of non-zero value. The field data for data stream packets from the device has unique description for every measurement field. For example, it can be set of 3 float numbers as in accelerometer vector data or hexadecimal and floats as in compensated angular rate.

The checksum of the packet includes two bytes presenting a sum of all bytes in a packet except themselves calculated using Fletcher checksum algorithm for hexadecimal number notation. The checksum algorithm is presented in LabVIEW subVI for packet generation on a **Figure 23**.

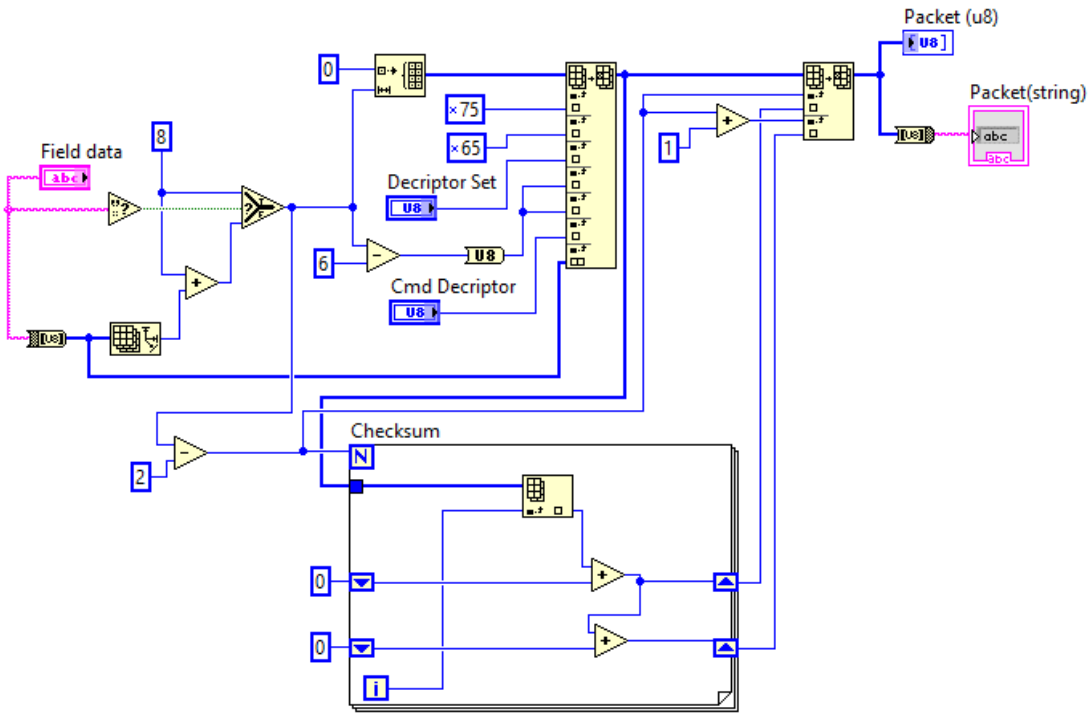

Figure 23. Packet generator for inertial sensor.

The developed algorithm allows to create packets automatically just by setting input descriptor set, command descriptor and field data values. This program is used as a subroutine block in the main code. Aside from the packet generator, a packet parser program was implemented to the main LabVIEW platform. Design of that subVI is because streaming data from the serial port in LabVIEW goes without pauses between packets. Moreover, the serial port data comes to the program in string format but for processing it is compulsory to translate it into hexadecimal numerical format. For all these purposes, the packet parser code was made. It can be divided into logical blocks: packet separation, payload length control and packet payload generator are demonstrated in a **Figure 24**.

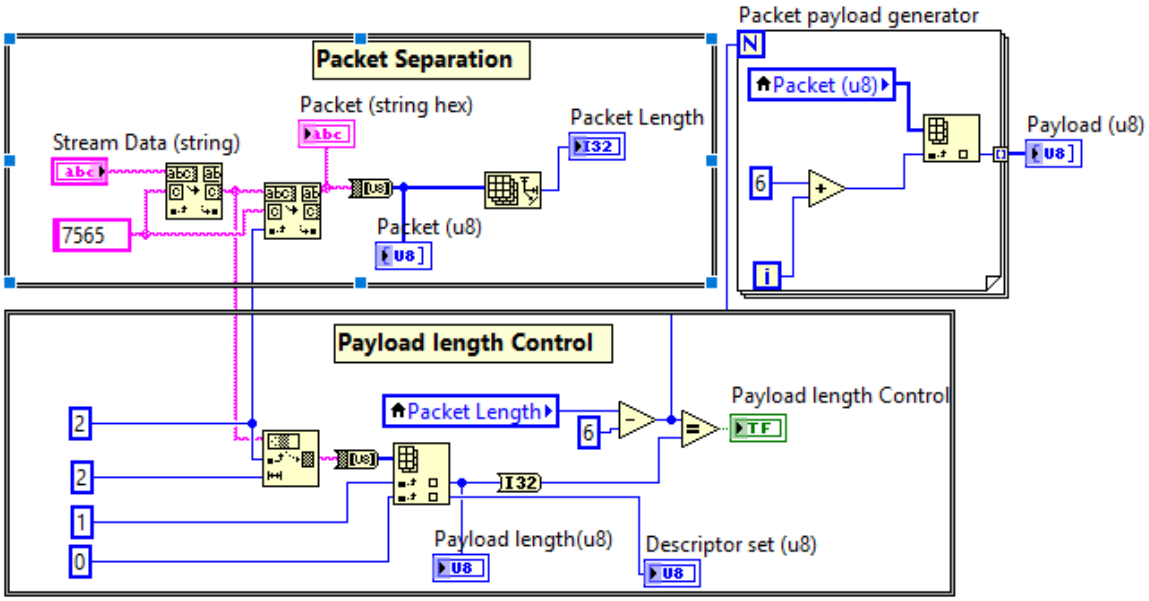

Figure 24. Packet parser for the inertial sensor. Part 1.

The packet separation part searches for beginning of adjacent messages in the data stream and writes packet information to the arrow of hexadecimals bytes. The next step of the packet parser is the check of quantity of bytes in the payload of the packet. Payload length byte from the packet is compared to the number calculated by the program. If it is true, payload length control diode will be turned on. The last block of that part is packet payload generator, which separates payload values from the whole packet array. That part of code is used later as a function block in the main code.

The second part of the packet parser shown on a **Figure 25** is a checksum control. It is needed in case if previous check was right just occasionally and payload from one packet was the same length as the value of byte representing payload length from the other packet. Checksum control estimates the Fletcher checksum value and compares it with two last bytes of the packet. In case of concurrency checksum control diode changes its state to ON.

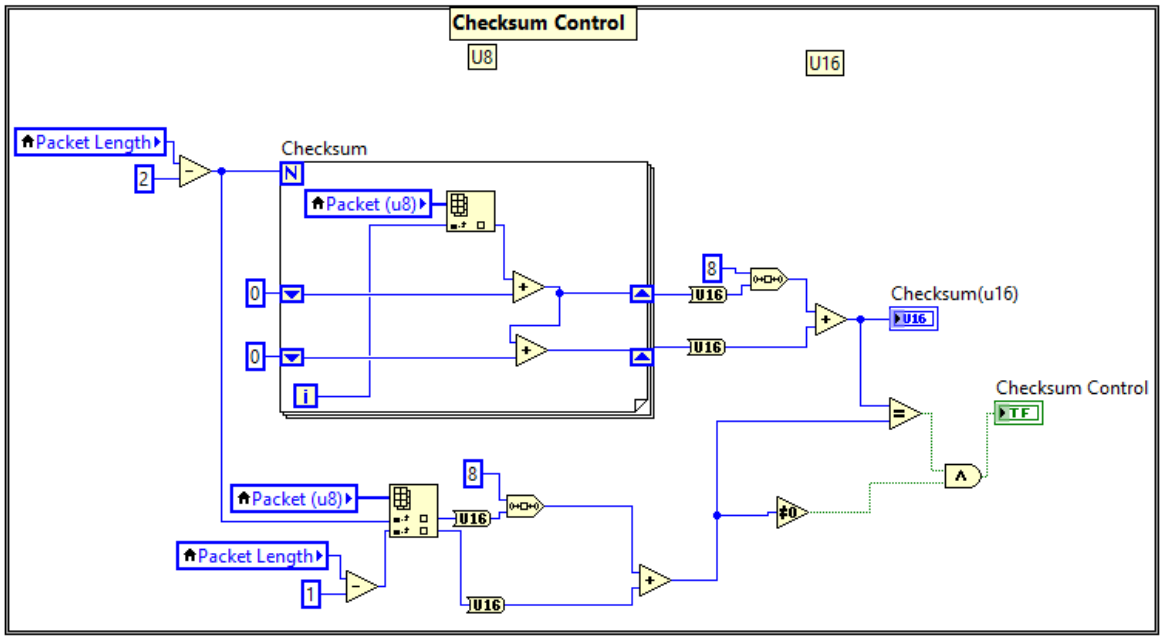

Figure 25. Packet parser for the inertial sensor. Part 2.

Merging of all values received on those steps takes place after two first parts of the packet parser. Cluster generation given on a **Figure 26** runs just after complete execution of previous parts.

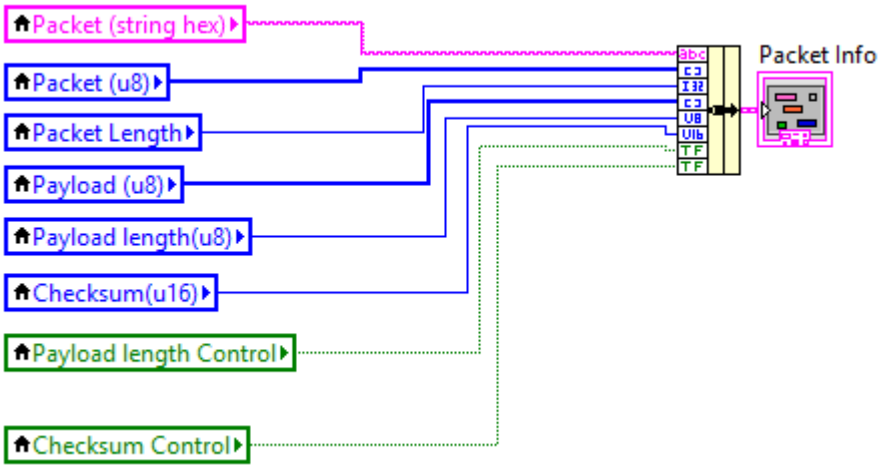

Figure 26. Packet parser for the inertial sensor. Part 3.

There are two ways of work with the INS: receiving stream-data packets with information from sensor and polling device, which means sending one command and receiving one reply per request. For both approaches, the sensor has to be configured beforehand. Configuration of the sensor includes some stages, which are integrated in the program as sequence parts, running one by one. First stage is opening of a serial port connection (**Figure 27**).

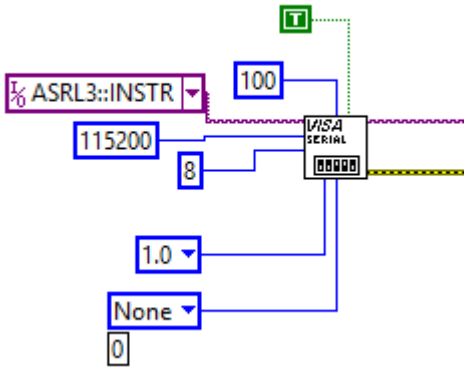

Figure 27. Opening of the serial port communication with the inertial sensor.

For that purpose, the block Configure Serial Port from the Serial Data Communication library is used. Important inputs of it are a resource name, which is similar to the name and number of the cRIO serial port where the sensor is connected to; baud rate is a rate of sending and receiving of the information (by default the sensor baud rate is 115200); data bits characterize how many information bits will be in one message.

Further, each stage operates owing to implementation two blocks from Serial Data Communication library: Write and Read, and comparison of the reply message after the Read block with the expected packet. The Write is used for sending command to the sensor, the Read receives signal from the device. The Packet Generator block described above is placed before the Write block and the Packet Parser in its turn follows the Read block. Framework of each stage of configuration process is almost the same, but there are some additional algorithms in some of them.

The second stage after configuration of the serial port is sending Set to Idle command. It disables all streams from sensor if they were turned on before. Most probably, they were enabled previously, because enable is a default state. Moreover, streams can work if before the sensor was shut down incorrectly. The third stage is a configuration of IMU message format. The forth is a configuration of Estimation Filter message format. Next stage is saving of all previous settings. Then it has to be chosen one option of work with sensor: streaming or polling. If operator decision is to get a stream from the sensor then next step is to enable a stream. If opposite, the last stage of initial settings is to start polling process.

For that application it is preferably to receive the continuous data stream from the device to have constant information about present state of the system. In the end of the work with the robot the program has to be shut down and serial connection has to be closed. For that purpose, the last step of the communication procedure with the sensor is closing the serial communication connection. The final sequence of the process for the inertial sensor control section of the main LabVIEW program is demonstrated on a **Figure 28**.

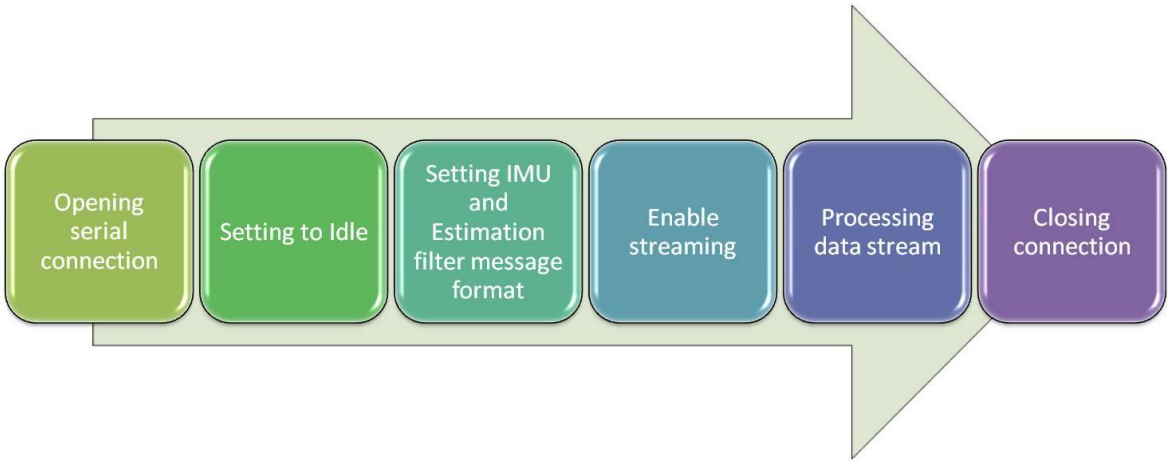

Figure 28. Sequence of inertial sensor section work.

It was detected that it is very difficult to analyze packets from different data sets, because they have different length. Length of the read information from serial port is an input for block Read from serial port in LabVIEW and it has to be set beforehand. If packets have different length, it generates shifts of data and losing synchronicity and as consequence valuable data. That is why the work with different data sets should be managed separately.

Moreover, content of one stream-data packet is very important. There are plenty of different variables for every data set. It is not possible to request all of them in one packet. Hence, the most important variables are determined and further data analyze work is made just with them. These variables are linear acceleration in three axes, angular velocity around all axes and Euler angles. They were chosen due to further possibility of usage them in a solution of navigation problem. The sensor has option of position detection in space, but it works just with participation of the GNSS, which is not possible to use inside the building- anticipated robot environment.

Thus, the section of the data stream analysis presented on a **Figure 29** includes Read from serial port block, then abovementioned subVI Packet parser and algorithm for processing payload from the packet. The payload contains three fields: acceleration, angular velocity and Euler angles. Acceleration data is a set of three float values written in hexadecimal representation. Gyroscope values and Euler angles have the same structure of the payload data field. Following code shows the approach of translation of incomprehensible numbers and letters into numerical values of real measurements and graphical interpretation of them.

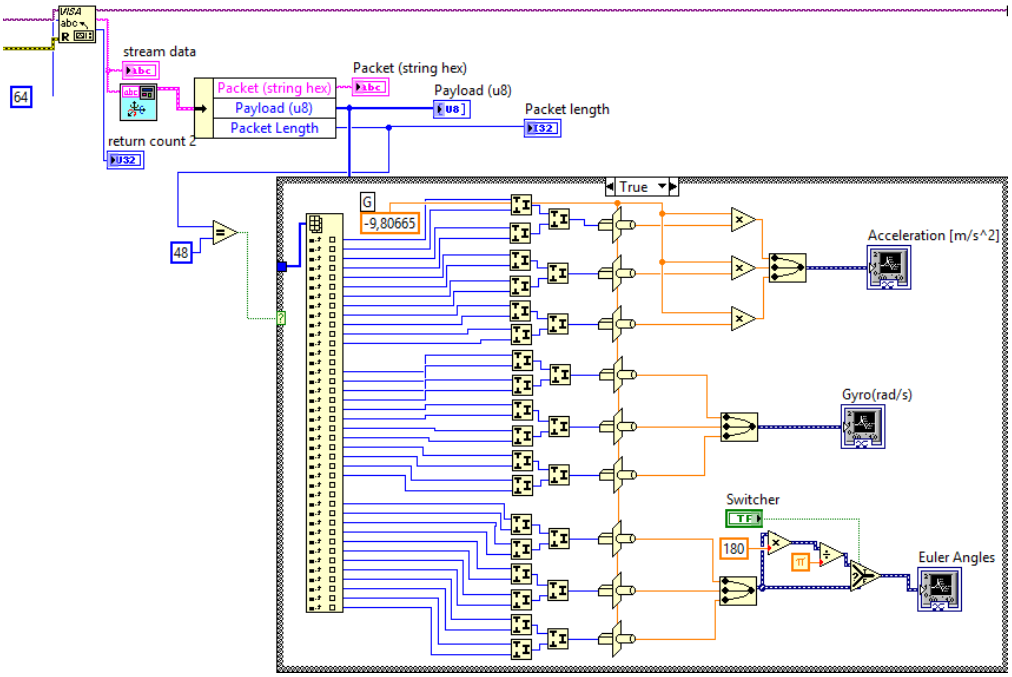

Figure 29. Data stream analysis.

It is worth nothing that Extended Kalman filter as Estimation filter of the sensor is applied to each measurement inside the sensor. Moreover, there are different approaches to configure it settings. The easiest method is send command of automatic initialization of the filter that is allowing the device processor decide what algorithm to use and which initial values include in calculation of the filter. Another possibility is sending settings about initial values and expected errors in command to the device. This option provides more flexibility to developer but probability of inaccuracy is increasing. Based on these considerations authorization of the Kalman filter for all device measurements is made automatically by the embedded algorithm after sending the command of running that code in the INS.

In conclusion, usage of different methods allows to combine hardware of the system with the software and to receive desirable result. Physical principles of changing electricity parameters with the changing of environment and the robot characteristics are bases for sensor system. Methods of measuring these varying values are applied to transformation of real word information into digital signal, where algorithms and program modeling work. The development of the desired computer interface platform targeted on a work with hardware devices would not be possible without program software LabVIEW, NI hardware controller, and reconfigurable input/output modules.

4 RESULTS AND ANALYSIS

The main result of the thesis is the organization of connection between hardware low-level subsystems and software control and monitoring system. The block diagram on a **Figure 30** demonstrates developed communication inside the system. The whole system is under control of the main station, where the LabVIEW program interface is launched. At the same time, the program is running on the cRIO controller onboard the mobile robot. The controller is connected with sensor and devices system and receives information from them which is by chain arrives to the remote control station and can be managed by an operator.

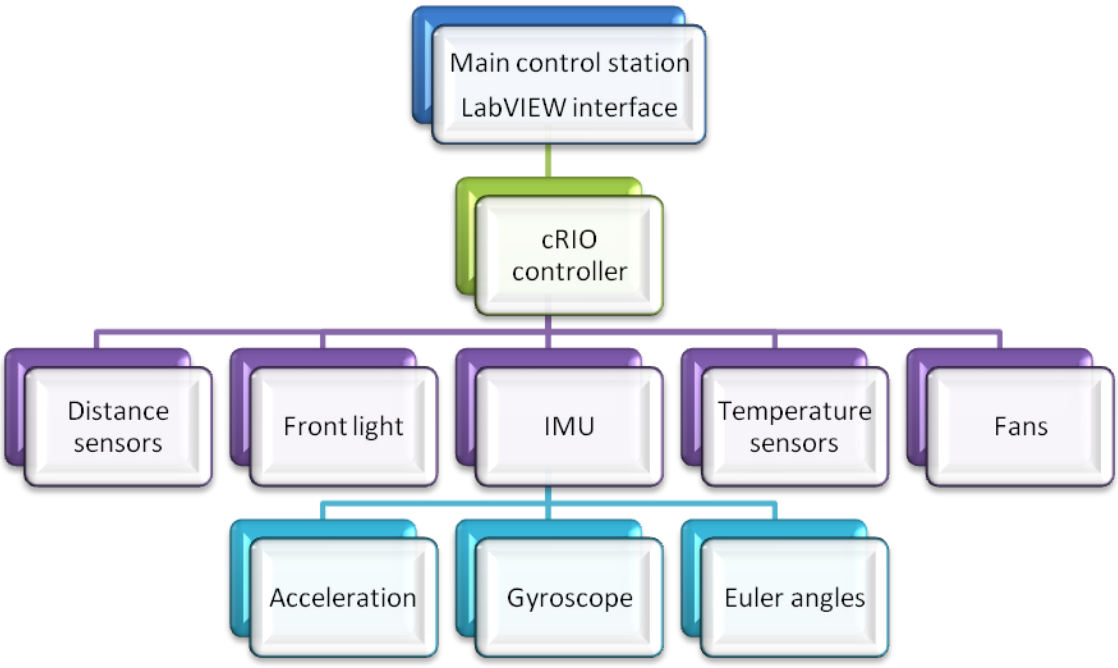

Figure 30. Communication diagram of the lower level subsystem.

During the development of the thesis, principles of work of temperature and distance sensors were studied as well as IMU with estimation filtering system for eliminating accumulating errors. The robot cooling system based on monitoring of the temperature under the robot cover was developed in the LabVIEW software. In addition, obstacle detection system using data from 8 distance sensors and front light control were implemented in the main program.

Packets of commands and data of INS were researched and analyzed. SubVI programs of packet parser and packet generator were made. Besides, two ways of work with inertial sensor were studied and streaming data type was chosen for the implementation in the project. Sequence structure of configuration setting of the inertial sensor was designed. Moreover, the INS measurement results were integrated in the main code and accelerometer, gyroscope and Euler angle information is received on the main control station.

All abovementioned systems are united in one control and monitoring interface (Figure 31) for simplifying of the robot operator work. Access to low level subsystem structure of the Mobile Assembly Robot is available from the main computer.

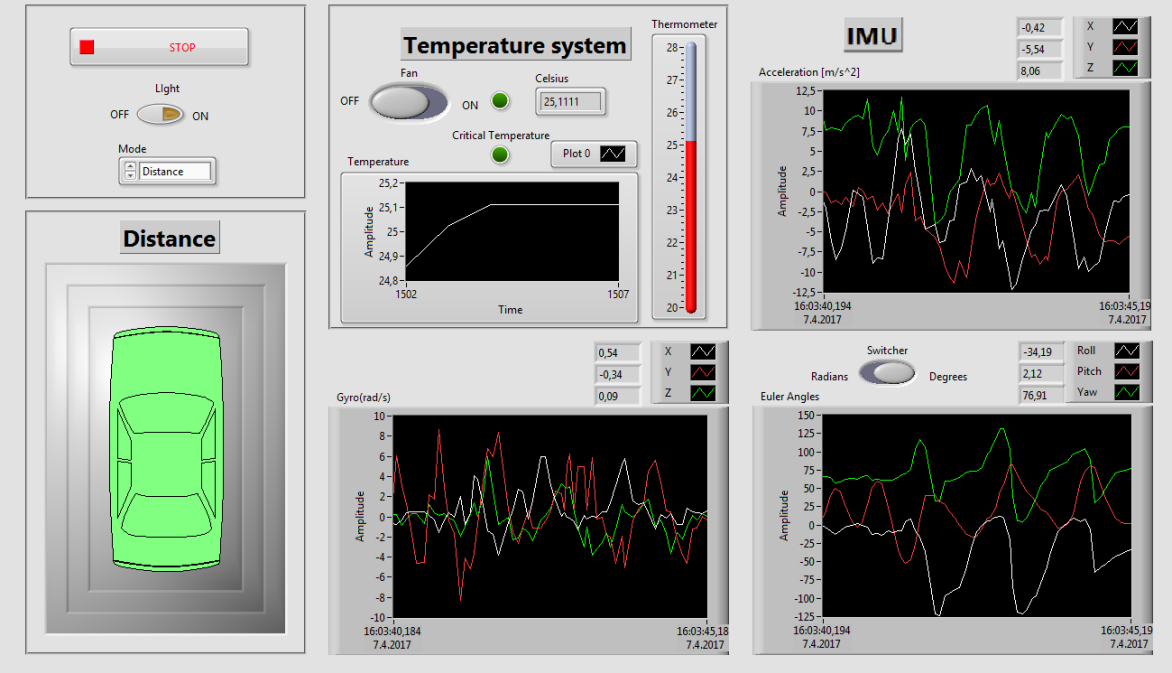

Figure 31. Developed platform interface in LabVIEW.

The whole developed system works very fast and stable. The demonstrative interface is easy to understand and utilize in the managing of other parts of the robot, for example, traction system or arms of the robot. In addition, developed system can be implemented into the ROS-based control system of the mobile robot.

5 CONCLUSION

Received result has a great importance for the Mobile Assembly Robot project, because the environment and the robot condition analysis in a hazardous area is one of the most required tasks for the remote control. The research question to that master thesis was if it was possible to develop a system combining different sensors subsystems with individual properties and features and provide people with an intuitive interface. It was proven in that work that answer on that question is positive. Problems of organization communication between hardware systems and software application occurred during the project, nevertheless, functions and properties of each device were considered in the implementation into the main LabVIEW platform to obtain the productive control system with the understandable interface.

Main aim of the research - the development of a platform for work with low-level subsystems, was achieved, but further researches are possible:

- Integration of the program into ROS control software,
- Modification of the code for improvement of the operation speed,
- Increasing flexibility of the interface, which will allow changing parameters and properties of devices.

In addition, it has to be noted that system can be modify with the aim of usage in different conditions. For example, developed system can be implemented into industrial robots application. Hence, other sensors or indicators can be added into designed code as well as they can replace utilized devices due to changes of the lower level subsystems purposes.

LIST OF REFERENCES

Childs, P.R.N., Greenwood, J.R. & Long, C.A. 2000. Review of temperature measurement. Review of scientific instruments, 71: 8. Pp. 2959-2978.

Chu, B. 2015. Mobile robot position control algorithm based on multiple ultrasonic distance sensors. Proceedings of the Control, Automation and Systems (ICCAS), October. 2015 15th International Conference. Pp. 1238-1240.

Comasolivas, R., Quevedo, J., Escobet, T., Escobet, A. & Romera, J. 2017. Modeling and Robust Low Level Control of an Omnidirectional Mobile Robot. Journal of Dynamic Systems, Measurement, and Control, 139:4, P. 041011.

Crone, W.C. 2008. A brief introduction to MEMS and NEMS. In: Sharpe, W.N. Springer handbook of experimental solid mechanics. USA: Springer Science & Business Media. 2008. Pp. 203-228.

Edwards, J. & Otterson, D. 2014. Tech Talk:(5) Temperature Measurement Basics. Measurement and Control, 47:9. Pp. 276-282.

Falsig, S. & Soerensen, A.S. 2010. An FPGA based approach to increased flexibility, modularity and integration of low level control in robotics research. Proceedings of the Intelligent Robots and Systems (IROS). October. 2010 IEEE/RSJ International Conference. Pp. 6119-6124.

Figliola, R.S. & Beasley, D. 2015. Theory and design for mechanical measurements. 6th ed. USA: John Wiley & Sons. 624 p.

Heller, E.B. & Youcef-Toumi, K. 2014. Analysis and control of a thermal management system for robots in temperature-restricted environments. Proceedings of the American Control Conference (ACC). June.2014. Pp. 3335-3340.

IEC 60751. 2008. Industrial Platinum Resistance Thermometers and Platinum temperature sensors.

Kalman, R.E. 1960. A new approach to linear filtering and prediction problems. Journal of basic Engineering, 82:1. Pp. 35-45.

Keyence Corporation. 2017. Comparison between Ultrasonic Sensors and Optical Sensors. [webpage]. [Referred 02.04.2017]. Available: http://www.keyence.com/ss/products/sensor/sensorbasics/ultrasonic/comparison/

King, A. 1998. Inertial navigation-forty years of evolution. GEC review, 13:3. Pp. 140-149.

Kuttruff, H. 2012. Ultrasonics: Fundamentals and applications. Springer Science & Business Media.

LORD MicroStrain. 2015. 3DM-GQ4-45 Data Communication Protocol [web document]. Published 2015, updated 26.09.2015 [Referred 08.4.2017]. Available: http://www.microstrain.com/Inertial/3dm-gq4-45.

LORD MicroStrain. 2016. 3DM-GQ4-45™ Compact, Tactical-Grade All-In-One Navigation. [webpage]. [Referred 05.04.2017]. Available: http://www.microstrain.com/Inertial/3dm-gq4-45.

Manu Systems AG. 2017. SRF06 Current Loop Ultra-Sonic Ranger with 4-20mA Output. [webpage]. [Referred 20.04.2017]. Available: http://en.manu-systems.com/DEV-SRF06.shtml.

Martin, J., Beck, S., Lehmann, A., Mikut, R., Pylatiuk, C., Schulz, S. & Bretthauer, G. 2004. Sensors, identification, and low level control of a flexible anthropomorphic robot hand. International Journal of Humanoid Robotics, 1:03. Pp. 517-532.

Maslov, A., Maslov, D. & Merkuryev, I. 2014. Studying stationary oscillation modes of the gyro resonator in the presence of positional and parametric excitations. Gyroscopy and Navigation, 5:4. Pp. 224-228.

Minco Components. 2015. Bolt-On and Economy Sensors: S102408PD3G40. [webpage]. [Referred 05.04.2017]. Available: http://catalog.minco.com/catalog3/d/minco/?c=products&cid=1_7_3-bolt-on-economy-sensors&id=S102408PD3G40.

National Instrument. 2014. [www- data sheet]. NI 9203. [Referred 05.04.2017]. Available: http://www.ni.com/en-gb/shop/select/c-series-current-input-module?modelId=122156.

National Instrument. 2016a. [www- data sheet]. NI cRIO-9035 Embedded CompactRIO Controller with Real-Time Processor and Reconfigurable FPGA. [Referred 05.04.2017]. Available: http://www.ni.com/en-gb/support/model.crio-9035.html.

National Instrument. 2016b. [www- data sheet]. NI 9217. [Referred 05.04.2017]. Available: http://www.ni.com/en-gb/shop/select/c-series-temperature-input-module?modelId=122169.

National Instrument. 2016c. [www- data sheet]. NI 9472. [Referred 05.04.2017]. Available: http://www.ni.com/en-gb/shop/select/c-series-digital-module?modelId=122223.

National Instrument. 2017a. CompactRIO Controller. [webpage]. [Referred 05.04.2017]. Available: http://www.ni.com/en-gb/shop/select/compactrio-controller.

National Instrument. 2017b. C Series Current Input Module. [webpage]. [Referred 25.04.2017]. Available: http://www.ni.com/fi-fi/shop/select/c-series-current-input-module?modelId=122156.

National Instrument. 2017c. C Series Digital Module. [webpage]. [Referred 25.04.2017]. Available: http://www.ni.com/fi-fi/shop/select/c-series-digital-module?modelId=122223.

National Instrument. 2017d. C Series Temperature Input Module. [webpage]. [Referred 05.04.2017]. Available: http://www.ni.com/en-gb/shop/select/c-series-temperature-input-module?modelId=122169.

National Instrument. 2017e. NI-9870 (C Series Serial Instrument Control Module). [webpage]. [Referred 27.04.2017]. Available: http://www.ni.com/en-gb/support/model.ni-9870.html.

Pallàs-Areny, R., Webster, J.G. & Areny, R.. 2001. Sensors and signal conditioning. 2nd ed. Toronto,Ontario: John Wiley & Sons. 587 p.

Qazizada, M. E. & Pivarčiová, E. 2016. Mobile Robot Controlling Possibilities of Inertial Navigation System. Procedia Engineering, 149. Pp. 404-413.

RdF Corporation. 2003. PLATINUM RTD Probe Construction. [webpage]. [Referred 05.04.2017]. Available: http://www.rdfcorp.com/anotes/pa-r/pa-r_01.shtml.

Scopus, 2017. Analyze search results.Year. [web database]. [Referred 02.04.2017]. Available: https://www-scopus-com.ezproxy.cc.lut.fi/term/analyzer.uri?sid=23DE18817DF389DE2FB4483A239AA561.wsnAw8kcdt7IPYLO0V48gA%3a20&origin=resultslist&src=s&s=TITLE-ABS-KEY%28low+level+control+AND+robotics%29&sort=plf-f&sdt=b&sot=b&sl=45&count=1836&analyzeResults

Siciliano, B. & Khatib, O. eds. 2016. Springer handbook of robotics. Springer.

Siciliano, B., Sciavicco, L., Villani, L. & Oriolo, G. 2010. Robotics: modelling, planning and control. Springer Science & Business Media.

SunonWealth Electric Machine Industry Co. 2016. [www- data sheet]. Specification DC Brushless Fan PMD2412PMB1-A.. [Referred 20.04.2017]. Available: http://portal.sunon.com.tw/pls/portal/sunonap.sunon_html_d_pkg.open_file?input_file_name=7264646F632F3230313430312F3137373830342F5F443132303036333430472D30305F2D332E706466.

Terzic, J., Terzic, E., Nagarajah, R. & Alamgir, M. 2013. Ultrasonic fluid quantity measurement in dynamic vehicular applications. Switzerland: Springer International Pulishing.

Trusov, A. 2011. Overview of MEMS gyroscopes: history, principles of operations, types of measurements. Irvine, USA: University of California.